

FAULT LOCATION: THE MODELS, METHODS, AND SOLUTIONS

1. INTRODUCTION

Determining fault location in power systems using the available measurements and models is an important task since it allows the maintenance crews to inspect the site where the fault may have occurred, inspect the equipment, make repairs, and allow the operators to restore the service. This task has evolved over time regarding the proposed methods and available engineering tools. This article is a survey of some of the very original methods that were introduced when digital technology was applied to power systems over 40–50 years ago as well as some very new methods introduced in the past few years. Covering a span of over 50 years allowed us to mention only some of the details of the most promising approaches, while many details had to be left to the readers' personal efforts in reading a comprehensive list of references provided at the end.

The organization of the article is as follows: the fault location background, basics of fault location algorithms, and approaches to determining transmission line model parameter are covered in the first three sections. We then cover the fault location methods based on the measurements of the waveforms reflecting electromagnetic transients, phasors, and electromechanical transients in Sections 4–6, respectively. We finally cover the algorithms based on a combination of physics- and data-based methods used for determining fault location in distribution systems in Section 7, and predicting faults in both transmission and distribution systems in Section 8. Conclusions are given in Section 9, followed by references in Section 10.

2. THE FAULT LOCATION BACKGROUND

Power systems represent a vital component of the electrical utility infrastructure aimed at supplying power to a variety of users. These systems consist of a number of different components including generators, power transformers, transmission lines, and loads. The design of the system components and the overall systems is implemented under a stringent reliability requirement with a strong emphasis on continuity of the power supply.

The most common and desirable operating mode of a power system is the normal operation in which typically an alternating-current (ac) generator is used to produce and maintain the supply of the sinusoidal 60-Hz waveforms of voltages and currents. Transmission lines used to connect the generators and loads allow the transfer of power between the generation and load sites. Power transformers are used to step up the voltage from the generator level to the transmission-line level for more efficient transfer of power over the transmission lines connecting the generators and loads. At the location of the load, power

transformers are used again to step down the voltage to the levels required by a variety of loads. All or the major components in a power system are connected using switching equipment, allowing the components to be put in and out of services as needed.

Power-system operation can be viewed as falling into one of the following states: normal, emergency, or restorative. As in any other technical system, there are circumstances under which failures in the system operation do occur. The faults on a transmission line create an emergency operating state. They are detected by special equipment called protective relays. Protective relays are designed to issue a trip command to the switching equipment (circuit breakers) to open both ends of a transmission line if a fault is detected and confirmed by the relaying algorithm as being present on that line. Eighty to ninety percent of all faults are temporary. After a fault has occurred and relays have detected the fault and disconnected the line, it is a general practice to automatically attempt to restore the line one or more times. If the fault is gone when the line is reenergized, the circuit breakers will stay closed, and only a momentary loss of service occurs. Automatic reclosing is done between 30 cycles and 30 seconds, depending on the utility's practice. If the fault is permanent, the relays will trip the circuit breakers each time they reclose until the preset number of reclosures has occurred, at which time the circuit breaker is locked out and the line remains deenergized until the fault is inspected and damage repaired. In either event, it is important to determine the location of the fault. Even temporary faults may leave a residue of damage which must be repaired at the earliest opportunity. If the fault is permanent, the damage must, of course, be repaired and the line returned to service.

Fault-location techniques are used to determine the location of the fault on a transmission line or distribution feeder. Once the damage caused by the fault can be located, the line/feeder can be repaired and restored as soon as possible. Since the efficiency in repairing and restoring the line/feeder is greatly dependent on the ability to locate the damaged part accurately, it is extremely important that the fault-location algorithm is very accurate, so that the maintenance crews can be dispatched to the appropriate location immediately.

Most transmission-line or distribution feeder faults occur during severe weather conditions when lightning strikes towers or conductors, producing stresses on the insulation between the conductors and supporting structures. In addition, some natural environmental conditions such as a tree growing or bird flying into a transmission line or distribution feeder can cause a fault. The cause of the fault in this case is a foreign object connecting the cables causing the insulation breakdown. Since all of the mentioned causes are random, faults can occur at any time and at any location.

2.1. Properties of Conductor Faults

The transmission line or distribution feeders fed by an ac source are built with either three- or single-phase conductor configuration. Our discussion will be related to

a three-phase system. The three-phase system assumes that there are three conductors, each energized with currents and voltages. These conductors are mounted on towers/poles that support the line/feeder all the way from the generating plant or a substation to another substation or a customer load. The typical span between two transmission towers in a high-voltage transmission system is between 200 and 500 m. The spans between distribution poles are far shorter. The electrical relationship between the three-phase voltages or currents is represented with phasors that are of the same magnitude but 120° apart. These phasors can be defined for an electrical condition between each of the conductors or between a conductor and a ground potential. These quantities are typically called the line and phase values, respectively.

Transmission-line faults are mostly caused by deterioration of the insulating materials due to environmental and particular operating conditions. Construction of overhead transmission lines requires that the conductors carrying the current are dispensed on large supporting structures called towers or poles. Since the most common transmission principle uses three-phase systems, at least three conductors are placed on one supporting structure. To make sure that there is no insulation breakdown between the conductors and supporting structures, as well as among conductors, several insulating components and principles are used. Most commonly, ceramic or polymer insulators are used when connecting the cables to the supporting structure. In addition, adequate spacing between conductors is provided to allow for air to serve as an insulator between conductors. In some instances, a separate conductor connected to the ground at each of the supporting structures is placed on the top of the structures (the “earth” conductor). It is used to shield the other conductors from the impacts of lightning that may cause an insulation breakdown and damage the insulators and conductors.

Once a fault occurs on a conductor, it can take a variety of forms. The common fault is the connection of a conductor to the ground. This connection can be via an electrical path of very low resistance, such as an arc caused by a lightning strike. In most of the ground faults that are caused by a lightning strike, the connection with the ground is established via an earth wire placed on the top of the tower and connected to the ground at the footing of each tower. Yet another possibility is that the ground connection is established via an electrical path with a higher resistance, such as the case in which a tree or a foreign object provides the connecting path. These types of faults are called ground faults and can be established individually between any of the conductors and the ground or between any two conductors jointly connected to the ground. In addition, all three conductors can be involved jointly in a three-phase ground fault. The other types of faults are related to various combinations of faults between the conductors without involving a ground connection. These types are called phase-to-phase faults. It is important that fault-location techniques are capable of accurately determining the fault location under a variety of different fault types.

Yet another consideration associated with the fault is the length of time required to detect the fault and

disconnect the transmission line. As mentioned earlier, protective relays are used to detect a fault and issue a trip command to a breaker. There are two distinct time frames involved in fault detection and fault location. Protective relays may be required to operate very fast such as in one cycle 60 Hz, 1 cycle = 16.66 ms, in the case of transmission line fault clearing. To do this, relays are set to recognize whether a fault is in or out of a given zone of protection and to make the decision in the presence of electrical noise and other transient effects such as dc offset, current transformer, or potential transformer inaccuracies. The exact location of the fault is not required as long as it is determined that it is within the zone of protection. This operating time requirement of 1 cycle may result in an incorrect decision and an incorrect operation. The relay, however, must be dependable (when there is a fault, the relays trip) and secure (when there is no fault, the relays do not trip). In high-voltage and extra high-voltage networked systems this is acceptable because the power system itself is designed to be robust and maintains its integrity even with the loss of a line. At distribution and industrial voltage levels where the system is radial (i.e., only single source), security may be a more important factor than dependability since the loss of a line may result in the loss of service to an area or a group of customers. In this situation, the relay’s operating time may be delayed beyond 1 cycle to be sure that the measurement is correct. After the relay has operated and a trip command is given to the circuit breaker, the circuit breaker will clear the fault in 2–3 cycles, making the total clearing time 3–4 or more cycles. For fault location, this is the time that the current and voltage waveforms can be monitored.

Another aspect of a relay operation is the provision to reclose the circuit breaker automatically after it had been opened by the relay trip action. This technique is called automatic reclosing and is commonly applied on high-voltage transmission lines and in some special instances on the distribution feeders. Since quite a few of the transmission-line faults are temporary in nature, the autoreclosing function provides an automatic attempt to reclose the line and keep it in service if the fault has disappeared. Furthermore, the circuit breakers can operate on all three phases simultaneously, or the construction may allow for single-phase (single-pole) breaker operation. Fault-location techniques need to be able to determine the fault type correctly so that a proper autoreclosing action can be applied.

2.2. Fault Location Requirements

As an example, the transmission-line fault-location function needs to satisfy several major requirements as follows:

- The accuracy must be sufficient to locate the fault within a span of two towers. Typically, 0.1% error is acceptable, but an accuracy of 0.01% is desirable.
- The accuracy should be maintained even if only a short segment of the fault data from a distorted waveform is measured. Typically, it is required that no more than a few cycles of data are sufficient for the calculation.

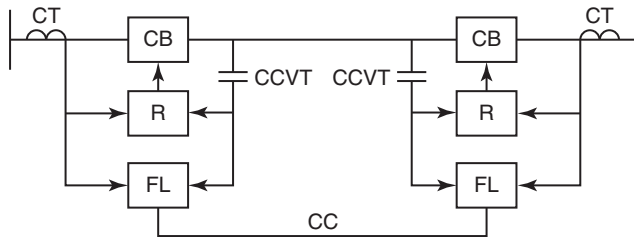


Figure 1. Fault-location equipment connection. CB is the circuit breaker, R the relay, FL the fault locator, CT the current transformer, CCVT the capacitor coupling voltage transformer, and CC the communication channel (not always required).

- The accuracy should not deteriorate if various types of faults and numerous autoreclosing requirements are considered. Typically, it is acceptable if the accuracy deteriorates under some difficult fault cases in which the fault resistance changes during the fault, but it is desirable that the accuracy be stable even under these conditions.

Fault-location application requirements are quite diverse and can be discussed using Figure 1.

Protective Relaying System. The fault-location application requires that full consideration is also given to the elements that constitute the relaying systems: protective relays, instrument transformers, and circuit breakers. Protective relays are supposed to detect the fault and isolate the line before the system is endangered and further damage is incurred. The fault clearing time of a typical transmission-line relay is around four cycles, which should provide sufficient measurement time to obtain the waveform data for the fault-location application. Since the relays give a determination based on the waveform measurements obtained by the current transformer and capacitor coupling voltage transformers (CT and CCVT, respectively), it is important to understand the errors introduced by the transformers. Typical distortion that may affect the current waveform is the saturation of the iron core. The CCVT are associated with low-pass filtering characteristics as well as signal oscillations in the case of voltage collapse. The instrument-transformer inaccuracies are very important in determining the overall error in the fault-location algorithm. The instrument-transformer error may significantly affect the fault location error, causing it to deteriorate for an order or magnitude. Finally, the circuit breakers are initiated by the relays to clear the fault. The phenomena of breaker restrike and ferro resonance distortion are important when using the waveform data captured before the breaker opens in calculating the fault location.

Implementation Requirements. The algorithms for fault location may be implemented using

- Fault-location devices
- Protective relays
- Digital fault recorders

Stand-alone fault locators are the most flexible option since the entire design can be optimized for fault-location application. At the same time, this is the most expensive solution since the entire device accommodates only one function, namely, the fault location. Some vendors have opted for such a solution, justifying an increased cost with a claim that their fault-location implementation guarantees unsurpassed accuracy performance (1).

The most common implementation approach is to use the line/feeder protection relays as the platform for the fault-location implementation. This approach is cost effective since the increment required to accommodate the fault-location algorithm is minimal. Almost all of the protective-relay vendors offer some form of a fault location algorithm as a standard feature of their relay designs.

Yet another option is to use a digital fault recorder (DFR) design as the platform for fault-location implementation. DFRs are commonly used in high-voltage transmission substations to record voltages and currents on the transmission lines. Again, most of the DFR vendors have implemented a fault-location algorithm and provide it as a standard feature of their product.

Even though fault-location implementation can be diverse, it should be noted that the accuracy and cost requirements are always the key consideration. Therefore, it is essential to understand the possible benefits and shortcomings of using different types of data and system-implementation approaches when designing or selecting a fault locator.

Cost/Performance Considerations. As an example, the following design considerations directly affect the cost/performance rating of a given fault-location implementation on transmission lines:

- One- or two-ended application
- Synchronized or unsynchronized data acquisition
- Data samples from the adjacent lines

The least expensive fault-location application is to use a single-terminal measurement of voltages and currents. In this case, an existing transmission line relay or a DFR can be used. The main difference between these application approaches is the input data waveform processing requirement. Most of the protective relays use a low sampling rate to reconstruct phasors. The DFR sampling is up to 5 kHz and higher and enables recovery of other waveform components. The accuracy and complexity of the input channels have a bearing on both the cost and performance of the fault-location implementation.

A more expensive but also more accurate solution is a two-terminal implementation with which the data from the transmission line ends are collected and brought to a centralized place where the fault location is calculated. In this case, a communication channel is needed to transfer the required data, which increases the cost of the overall solution. A variation between these solutions is in the way the data sampling is performed. Most of the implementations do not require that the data sampling at two ends of the line is synchronized to a common time source, while the most accurate solutions require the synchronization (2).

Finally, in order to achieve even greater fault-location accuracy, data samples from the lines parallel to the faulted line, and from all ends of a multiterminal line involved in a fault, can be used. Obviously, more input channels and communication facilities are needed in this case, but accuracy can be improved significantly (3).

3. THE BASICS OF TRANSMISSION LINE FAULT LOCATION ALGORITHM

A fault-location algorithm defines the steps needed to obtain the fault location using the measurements of voltages and currents from one or more ends of the line. A set of equations representing the mathematical model of the faulted transmission line is needed to define the algorithm. The quantities that appear in the equations are (i) voltages and currents, (ii) transmission-line parameters, and (iii) fault parameters.

The voltage and current in power systems are a combination of four kinds of signal components: fundamental, higher or lower frequency, transients, and noise. The fundamental component is a sinusoid having a system frequency that is equal to 60 Hz (in the United States or 50 Hz in some other countries). The higher or lower frequency components are also sinusoids having a frequency different from the fundamental one. The transients are temporary phenomena having diverse mathematical representation. They arise whenever the voltages or currents abruptly change. An occurrence of the fault causes such an event. The noise is a random signal component usually generated by measurement errors. In the normal operation of the transmission line, the fundamental component is dominant.

Two types of transmission-line mathematical models are in use for fault-location algorithms: the distributed-parameter model and the lumped-parameter model. The distributed-parameter model is mostly suitable for long transmission lines. The lumped-parameter model is a simplification of the distributed-parameter model and is used for shorter lines only. These models are also known as the long- and short-line model, respectively. Further details about the use of the models are given in Section 3.

In the distributed-parameter model, the voltages and currents are functions of time t and position r . The model consists of two linear partial differential equations of the first order. First, we consider the equations for the case of the one-phase transmission line:

$$-v_x(x, t) = li_t(x, t) + ri(x, t) \quad (1)$$

$$-i_x(x, t) = cv_t(x, t) + gv(x, t) \quad (2)$$

In these equations, the line parameters l , r , c , and g are inductance, resistance, capacitance, and conductance per unit length, respectively, $v(x, t)$ is the voltage, and $i(x, t)$ is the current. The subscripts x and t denote partial derivatives regarding the position and time, respectively.

A three-phase transmission line has as a model two-matrix equation similar to equations 1 and 2. The elements of the voltage vector are three-phase voltages, and the

elements of the current vector are three-phase currents. Transmission-line parameters are represented by matrices \mathbf{R} , \mathbf{L} , \mathbf{C} , and \mathbf{G} and are composed of self-resistance, mutual resistance, inductance, capacitance, and conductance. The details of the determining parameters of such a model will be presented later.

The lumped-parameter model neglects the line conductance g and capacitance c . The partial derivative of the current relative to position, in equation 2, is equal to zero in this case. Therefore, the current does not change along the line. The integration along the transmission line from one end (the sending end) to a point at a distance x from the sending end produces the following differential equation:

$$v_x(t) - v_s(t) = xri(t) + lx[di(t)/dt] \quad (3)$$

In equation 3, $v_s(t)$ is the voltage at the sending end, $v_x(t)$ is the voltage at a distance x from the sending end, and $i(t)$ is the current on the line. In the case of a multi-conductor line, the model is a matrix equation similar in form to equation 3. The line has a matrix model containing as its elements the self-resistance, mutual resistance, and inductances.

The Fourier transformation of equation 3 can be made if all the line parameters are constant. Furthermore, if the currents and voltages are the fundamental components, they will appear in the equation as phasors.

Note that due to the linearity of the equations, voltages and currents in both models may be replaced by their components.

For example, voltages or currents may consist of a fundamental component only or a transient component only. The classification of the existing fault-location algorithms depends on the line model and the signal component used. Most of the existing algorithms belong to two main groups:

- Phasor-based algorithms use the fundamental component of the signals only. The fundamental components then appear as phasors. The line model is usually the lumped-parameter model.
- Partial differential equation-based algorithms use transient components of signals and the distributed-parameter model of the line.

We will explain the underlying principles of the two groups using their exemplary algorithms.

3.1. Phasor-Based Algorithms

The phasor-based algorithms use a Fourier transform of equation 3 to model the line. The line is represented by its impedance per unit length $Z = r + j2\pi f_0 l$ and its length d . Figure 2 depicts the circuit model of the faulted line. There are three groups of quantities in Figure 2. The phasors of voltages and currents are known since they may be calculated from the signal samples. The transmission-line impedance Z and its length are also known from the line construction data. The fault position x , the fault impedance Z_F , and the fault voltage V_F are not known.

The aim of the algorithm is to find the unknown distance x to the fault. Two main steps in a phasor-based algorithm are (i) calculation of phasors from the signal samples

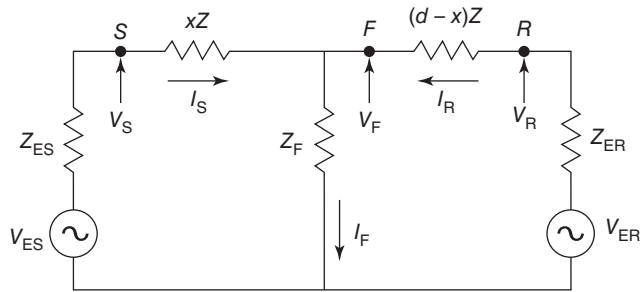


Figure 2. The circuit of a faulted transmission line. S , F , and R are the positions of the sending end, fault, and the receiving end, respectively; x is the distance to the fault; Z is the line impedance; d is the transmission line length; V_S , V_F , and V_R are the voltages at the sending end, fault, and the receiving end, respectively; I_S , I_F , and I_R are the currents at the sending end, fault, and the receiving end, respectively; Z_{ES} and Z_{ER} are the Thévenin equivalent impedances; and V_{ES} and V_{ER} are the Thévenin equivalent voltages.

and (ii) solution of the set of equations for the unknown fault distance.

The phasors are calculated from the corresponding voltage and current samples. An arbitrary sinusoid, say voltage $v(t)$, is represented by a phasor V . A phasor is a complex number defined by its real value $\text{Re}\{V\}$, its imaginary value $\text{Im}\{V\}$, or alternatively by its phase θ and amplitude $|V|$. The calculation of the phasor parameters is accomplished using Fourier analysis. The formulae for the real and imaginary parts of a phasor are

$$\text{Re}\{V\} = f_s \sum_{n=0}^{N-1} v(n/N f_0) \cos(2\pi n/N) \quad (4)$$

$$\text{Im}\{V\} = f_s \sum_{n=0}^{N-1} v(n/N f_0) \sin(2\pi n/N) \quad (5)$$

Here, N is an integer equal to the ratio of the sampling frequency f_s and the system frequency f_0 . The samples of the corresponding signal $v(t)$ are equal to $v(n/N f_0)$. They are taken in a window of samples one cycle long. The amplitude $|V|$ and the phase θ of the phasor are then calculated by the well-known formulae for the calculation of the amplitude and phase of a complex number from its real and imaginary values.

The preceding Fourier analysis formulae give an exact value of the phasor's real and imaginary values only if the signal is a pure sinusoid. The presence of the higher harmonics, transients, and noise introduces an error in the phasor calculation.

The phasor-based algorithms also differ depending on the location where the measurements are taken. One-end algorithms use measured data from one side of the line only. This side is conventionally named the sending end. Two-end algorithms use data from both the sending end and the other end, called the receiving end. One-end algorithms are more commonly used since they do not need the communication channel required in the two-end algorithms.

The One-End Algorithms. One of the well-known algorithms of this type was defined by Takagi et al. (4) for the three-phase transmission line. The fault type considered is the line to ground fault. This is the most common type of fault. For convenience, the fault was considered to be on phase a. The algorithm of Takagi et al. neglected mutual impedances and resistances between the phases. Therefore, the one-line diagram given in Figure 2 can be used to represent this case with the current and voltage coming from the phase only. Takagi et al. assumed that the impedance of the fault is a resistance equal to R_F . The equation relating the sending end voltage to the current and voltage at the fault follows from Figure 2:

$$V_S = xZI_S + R_F I_F \quad (6)$$

This is a complex scalar equation, equivalent to two real scalar equations. However, the number of unknowns is equal to four. One unknown is x , the phase and amplitude of the fault current phasor I_F are the other two, and the fault resistance R_F is the fourth unknown. The number of unknowns exceeds the number of equations, and additional equations are needed to calculate x . The second complex equation proposed by Takagi et al. represents an assumption about the currents of the receiving and sending ends. Each of these currents is the sum of a current existing before the occurrence of the fault (prefault current) and the superimposed fault current. These two components are denoted by a prime and a double prime, respectively. The sum of the prefault sending- and receiving-end currents is obviously equal to zero. Since I_F is the sum of the sending- and receiving-end currents, we have:

$$I_F = I_R + I_S = (I'_R + I''_R) + (I'_S + I''_S) = I''_R - I''_S \quad (7)$$

The circuit in Figure 2 is a current divider of the fault current. Thus, the sending-end fault current is equal to

$$I_S^n = \frac{[(d-x)Z + Z_{ER}]I_F^n}{dZ + Z_{ER} + Z_{ES}} = \frac{1}{k} I_F^n \quad (8)$$

Takagi et al. further assumed that all the impedances in the current divider of equation 8 have approximately the same phases. The consequence of this conjecture is that the fault current I_F is proportional to the sending-end fault current I_S^n . This means that the current distribution coefficient k in equation 8 is a real number. Based on the mentioned assumptions, the modified equation 6 follows:

$$V_S = xZI_S + kR_F I_S^n \quad (9)$$

Since the product of the current distribution factor k and resistance R_F may be seen as one unknown only, the number of unknowns is now equal to the number of equations. The fault location x is obtained by multiplying the modified equation with the conjugate of the sending-end prefault current denoted I_S^n and comparing the imaginary parts of the obtained equation:

$$x = \frac{\text{Im}(V_S + I_S^n)}{\text{Im}(ZI_S^n)} \quad (10)$$

There are several problems related to this approach. The first is the need to calculate the sending-end fault current I_S'' . Since this current in the postfault period is equal to the measured postfault current less the extrapolation of the prefault current, the recordings of the prefault current must be available. The other problem is related to the algorithm basic assumption. The neglected mutual coupling with other phases may be the source of error. Next, a current distribution factor that is a real number may be another source of error. Besides, one must know the faulted phase before the start of the calculation. These impediments may be resolved using symmetrical components and sequence circuits that are utilized to calculate short-circuit currents in three-phase networks. A brief review of this technique is given in the following section.

One-End Algorithms Using Symmetrical Components.

There are three symmetrical component phasors, zero sequence, positive sequence, and negative sequence, denoted as V^0 , V^1 , and V^2 , respectively, in the case of voltage. Each phase vector is a linear combination of these three components. During normal operation of the transmission line, zero and negative symmetrical components are equal to zero, and the phasor of phase a is equal to the positive-sequence phasor. Symmetrical components may be represented by a vector denoted \mathbf{V}^S . The vector of symmetrical components is obtained from the phase vectors by the following matrix equation:

$$\mathbf{V}^S = \mathbf{A}\mathbf{V}^P \quad (11)$$

Here, \mathbf{V}^P is the vector having as elements the phasors pertinent to phase a, phase b, and phase c. The matrix \mathbf{A} is given by

$$\mathbf{A} = \begin{bmatrix} 1 & 1 & 1 \\ 1 & \exp\left(\frac{j4\pi}{3}\right) & \exp\left(\frac{j2\pi}{3}\right) \\ 1 & \exp\left(\frac{j2\pi}{3}\right) & \exp\left(\frac{j4\pi}{3}\right) \end{bmatrix} \quad (12)$$

The equation defining the relation of the phase vector at the sending-end \mathbf{V}_S^P , the phase vector at the fault \mathbf{V}_F^P , the phase current vector \mathbf{I}_S^P , and the impedance matrix \mathbf{Z}^P is similar in form to equation 6:

$$\mathbf{V}_S^P = x\mathbf{Z}^P\mathbf{I}_S^P + \mathbf{V}_F^P \quad (13)$$

The impedance matrix \mathbf{Z}^P has mutual impedances and resistances at its off-diagonal terms. When the phasor vectors are replaced by the symmetrical component vectors, one gets

$$\mathbf{V}_S^S = x\mathbf{Z}^S\mathbf{I}_S^S + \mathbf{V}_F^S \quad (14)$$

The matrix \mathbf{Z}^S here is equal to

$$\mathbf{Z}^S = \mathbf{A}^{-1}\mathbf{Z}^P\mathbf{A} \quad (15)$$

While the matrix \mathbf{Z}^P has both the diagonal and off-diagonal elements, the off-diagonal elements of the matrix are all equal to zero. Hence, the matrix in equation 14 may be broken into three independent scalar complex equations:

$$\mathbf{V}_S^k = xZ_{kk}^S I^k + V_F^k \quad k = 0, 1, 2 \quad (16)$$

Here, Z_{kk}^S is the corresponding diagonal element of the matrix \mathbf{Z}^S . The main advantage of the symmetrical component application is this decoupling. Each of the decoupled equations defines a sequence circuit. They are called the positive-, negative-, and zero-sequence circuits. Since three decoupled equations have the same form as equation 6, the circuit in Figure 2 may again represent any of the sequence circuits with a suitable change in notation.

The previously mentioned obstacles of the Takagi et al. method are eliminated using the symmetrical components in the line model (5). In this approach, the negative-sequence circuit of the line is used. The decoupling feature of the symmetrical components eliminates the mutual inductance influence. Since the negative-sequence vector is equal to zero in the prefault condition, the recordings of the prefault current are not necessary as in the algorithm of Takagi et al. Moreover, according to these authors, the equivalent impedances and the line impedance of the negative-sequence circuit that make up the current divider are more likely to have the same phases than in the case of the phase impedances of the line (5). This implies that the assumption that the current distribution factor is a real number is close to reality. Also, the classification of the fault type before the calculation is not necessary. However, the exclusive use of the negative-sequence representation has a drawback. In the (very rare) case of a symmetric fault, the negative-sequence phasors after the fault remain equal to zero, and the negative-sequence circuit is not suitable for fault location.

The one-end algorithms require relatively simple calculations, and their implementation is opportune, since the waveform data are necessary from one side of the line only. They assume that the fault impedance Z_F is a constant during the fault. Their accuracy depends on the simplifying assumptions. In the case of a high fault impedance, the fault current is small; hence, the fault components of the sending-end current are very small. Since the fault current for the sending end is in the denominator of equation 9, the system is ill-defined in this case, and errors may be large.

Two-end algorithms require fewer simplifying assumptions and offer potentially more accurate calculations.

3.2. The Two-End Algorithms

Two-end algorithms fall into two subgroups: algorithms developed using synchronized samples and those developed using nonsynchronized samples. The samples are synchronous if the two data sampling clocks at the sending and receiving ends ensure that the samples are taken at exactly the same moments. This may be achieved by global positioning system (GPS) of satellites using clock signal pulse sent from a GPS satellite to tune two GPS receivers that synchronize the sampling clocks (1). This approach introduces additional cost to provide GPS receivers and appropriate waveform sampling interfaces. The impact of synchronization will be explained next.

One must note that phasors are calculated locally. If there is a time shift between the data acquisition clock pulses at the receiving and sending ends, the relative phases of the receiving and sending end phasors are not

the same. The phase difference between two phasors cannot be calculated by subtracting one phase from another. Suppose that the phasor at the receiving-end voltage is calculated from two sets of samples. The first set is taken using the sample clocked by the sending end. The resulting phasor is denoted as V_F . The second voltage phasor denoted as V'_F is calculated using the receiving-end clocked samples. If there is a time shift Δt between the two sets, the phases of the two phasors will differ for $\delta = 2\pi f\Delta t$. This may be mathematically expressed in the following way:

$$V_F = V'_F e^{j\delta} \quad (17)$$

The phase shift δ restates the nonsynchronized phasor (obtained using the data from the receiving end) to the frame reference of the sending end. This phase shift is the same for all voltages and currents, but it is not known in advance. Note that the phasor in both the time references has the same amplitude. The two-end methods consider the phase shift δ as an additional unknown and try to solve for the fault distance x by eliminating δ . Note that the sending-end voltage phasor calculated is V_S , and the receiving-end voltage and current phasor calculated locally are V'_R and I'_R , respectively.

An example of an algorithm using nonsynchronized samples is presented in Reference 6. The line model is constructed using a negative-sequence diagram. By inspecting Figure 2 and interpreting all phasors as negative-sequence phasors and all the impedances as negative-sequence impedances, the application of the Kirchhoff's voltage Law renders

$$V_F = V_S - ZI_S \quad (18)$$

$$V_F = V'_R - (d - x)Z_R I'_R \quad (19)$$

Since the absolute value of the fault voltage in both equations is the same, one gets the fault voltage $|V_F|$ from equations 18 and 19:

$$|V_S - xZI_S| = |V'_R - (d - x)ZI_R| \quad (20)$$

This is quadratic equation with respect to x , and it may be easily solved.

Two-end algorithms using synchronized samples start from the matrix equivalents of equations 18 and 19. Since all the phasors are calculated using the samples clocked at the same time, derived from the same clock, the two equations may be combined together. When the fault voltage is eliminated from these two equations, the following matrix equation follows:

$$V_S - V'_R - xZI_S + (d - x)ZI_R = 0 \quad (21)$$

This equation is equivalent to six real scalar equations. Since there is only one unknown x , the system is overdetermined. One alternative in such a situation is to use only a sufficient number of equations as in Reference 7. Another option is to use the minimum least squares (MLS) technique. The MLS technique is often used to identify parameters of a linear system using measurements corrupted with Gaussian noise (8).

The basic idea of the MLS method is to compensate for measurement errors using more equations than necessary and thus decreasing the measurement-error effects by averaging. The solution attained by the MLS method should not exactly satisfy any of the equations. When the MLS solution is put into the equations, the right-hand side of each scalar equation will not be zero but rather will be equal to a quantity of the error. The solution offered by the MLS method guarantees that the sum of all the squared errors will be the smallest possible. The matrix equation 19 in the MLS technique is represented as

$$\mathbf{A}x + \mathbf{B} = \mathbf{E} \quad (22)$$

where vectors \mathbf{A} and \mathbf{B} are defined as

$$\begin{aligned} \mathbf{A} &= -Z(I_S - I_R) \\ \mathbf{B} &= V_S - V'_R + ZI_R \end{aligned} \quad (23)$$

Here, \mathbf{E} is the vector of errors. The solution for x provided by the MLS technique minimizes the criterion function $J = \mathbf{E}^T \mathbf{E}$, and it is given by

$$x = -(\mathbf{A}^T \mathbf{A})^{-1} (\mathbf{A}^T \mathbf{B}) \quad (24)$$

The superscript \mathbf{T} denotes matrix transpose.

This method applied in Reference 7 requires more calculations but offers an increase of precision if there is significant noise in the measurements.

In conclusion, the phasor-based methods start from the fundamental assumption that all the transmission-line and fault parameters are constant during the fault and that the transmission line is homogeneous between the sending and the receiving ends. These assumptions may not be satisfied in some instances like when the value of the fault impedance changes in time if there is an arcing fault.

Also, the line may be compensated by inserting a series capacitor into the line, or there may be load taps between two-line ends. In addition, neglecting the line capacitance may introduce significant errors for a longer transmission line.

However, the most important issue in the phasor-based algorithms is the need for phasor estimation. Since in reality there is usually a decaying dc component and noise in the signal, phasors calculated using the Fourier analysis-based formulas given by equations 4 and 5 will differ from their true values.

The methods based on the distributed line parameters solve some of these problems. Calculation of phasors is not needed. The line capacitance is included in the model. The change of the fault impedance is not a problem, and these methods work if a series capacitor is inserted into the line.

4. DETERMINING PARAMETERS OF TRANSMISSION LINE MODELS

In this section, we first present the common transmission line constructions, then elaborate the commonly used short- and long-line models, and then present line parameter estimation methods for transposed lines.

4.1. Transmission Line Construction

- Long and short lines with different voltage levels (electrical properties of the line are associated with its length and voltage).
- Transposed and untransposed lines (line transposition is done by changing the relative position between conductors at a given tower, altering by this the symmetrical relationship between currents and voltages).
- Lines with mutual coupling (the mutual coupling takes place between conductors through an electromagnetic field and affects the electrical conditions on the conductors, in particular for the faults involving ground).
- Multiple line-per-tower construction (this is the case in which several sets of three-phase conductors, each representing several lines, are tied to the same tower, causing mutual coupling among conductors of different lines).
- Radial lines (lines that are directly connected to a single source of power).
- Series-compensated lines (lines that have capacitors connected in series with the line conductor).
- Lines with load taps (the loads are connected either directly or through a transformer to a line at any position along the line without using common switching equipment).
- Single- and three-phase lines (single- or three-phase conductors).
- Time-varying fault resistance (due to the breakdown of the insulation, the fault resistance changes during the fault disturbance).
- Changing prefault load conditions (the line may have distinctively different load current at a different moment of a fault).

4.2. Types of Transmission Line Models

Transmission line models are essential in fault location algorithm formulation and solution. Having accurate line models is pivotal for accurate fault location. Transmission lines are classified into short lines (<50 miles), medium-length lines (50–150 miles), and long lines (>150 miles). Accordingly, there are three commonly used line models: the lumped parameter model for short lines, the nominal-PI model for medium-length lines, and distributed parameter line model for long lines. These models are illustrated as follows.

The distributed parameter model consists of distributed series resistance, inductance, and shunt capacitance of line and is needed for analyzing traveling wave phenomenon. The shunt conductance is negligible. For steady-state analysis, the equivalent PI circuit model considering the distributed parameter effects is usually used, as depicted in Figure 3 (9). Z represents the equivalent series impedance of the line, and Y is the equivalent shunt admittance of the line. Let z_1 and y_1 denote the positive sequence series impedance and shunt admittance per unit length, respectively. The series impedance consists of

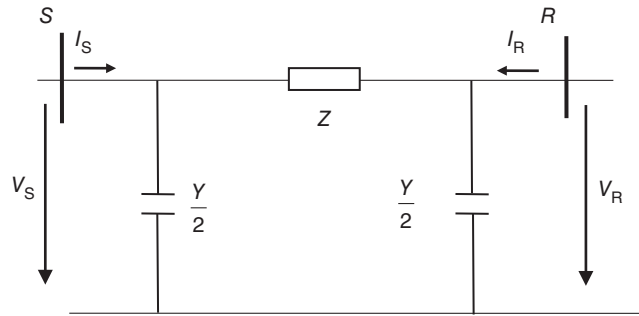


Figure 3. Equivalent PI circuit of a transmission line. Source: Jiao and Liao (9).

series resistance and inductance. Let Z_c be the characteristic impedance of the line, γ be the propagation constant of the line, and l be the total length of the line. The figure also shows sending and receiving end voltages and currents V_S , I_S , V_R , and I_R , which will be used to estimate the line parameters in the following section. All the quantities are for positive-sequence value. Then, we have

$$Z_c = \sqrt{z_1/y_1} \quad (25)$$

$$\gamma = \sqrt{z_1 y_1} \quad (26)$$

$$Z = Z_c \sin h(\gamma l) \quad (27)$$

$$\frac{Y}{2} = \frac{\tan h(\gamma l/2)}{Z_c} \quad (28)$$

The nominal PI model for the medium-length line takes the same form as shown in Figure 3, except Z and Y , which are calculated as follows:

$$Z = z_1 l \quad (29)$$

$$\frac{Y}{2} = \frac{y_1 l}{2} \quad (30)$$

For the short-line model, the model will only contain the series impedance Z , with the shunt admittance Y being omitted.

These models provide the basis for fault location algorithm development. The equivalent circuit model as shown in Figure 3 has been extensively used in impedance-based fault location methods based on phasors. Traveling wave and partial differential equation-based methods will need to use the distributed parameter line model. Regardless of which model is used, the parameter values including the series resistance, inductance, and shunt capacitance are essential inputs. These parameters are traditionally calculated based on the design parameters such as the conductor type, the tower structure, and the assumed temperature (10). However, the actual values may deviate from these calculated values due to varying environmental conditions and conductor operating conditions. Hence, it is desirable to develop methods to estimate the line parameters in real time using appropriate measurements (11–14). The following section provides two methods for estimating the line parameters based on real-time measurements.

4.3. Line Parameter Estimation Methods

This section presents two methods, that is, the least squares and the Kalman filter methods, for estimating the positive-sequence line parameters including the series impedance and shunt admittance per unit length based on synchronized positive-sequence voltages and currents taken at the two terminals of a line during normal operation. Although not shown, it is expected that zero-sequence line parameters can be estimated similarly if zero sequence measurements are recorded during unbalanced operation and fault conditions.

Least-Squares Method. Let us assume that there are N sets of synchronized measurements available at the sending and receiving ends (9). The measurement vector and matrices are defined as

$$\mathbf{A} = [I_{S1}, I_{R1}, \dots, I_{SN}, I_{RN}]^T \quad (31)$$

$$\mathbf{H} = \begin{bmatrix} V_{S1} & V_{R1} \\ V_{R1} & V_{S1} \\ \vdots & \vdots \\ V_{SN} & V_{RN} \\ V_{RN} & V_{SN} \end{bmatrix} \quad (32)$$

where superscript T denotes matrix transpose. Then, the following equation links the measurements and the line parameters to be estimated:

$$\mathbf{A} = \mathbf{H}\boldsymbol{\beta} \quad (33)$$

where $\boldsymbol{\beta} = [a, b]^T$, $a = \frac{Y}{2} + \frac{1}{Z}$ and $b = -\frac{1}{Z}$.

$\boldsymbol{\beta}$ is obtained based on the least-squares method as

$$\boldsymbol{\beta} = (\mathbf{H}^T \mathbf{H})^{-1} \mathbf{H}^T \mathbf{A} \quad (34)$$

Once $\boldsymbol{\beta}$ is calculated, Z and Y are obtained as

$$Z = -1/b \quad (35)$$

$$Y = 2(a + b) \quad (36)$$

Then, the series resistance, inductance, and capacitance can be further derived based on equations 25–28.

Kalman Filter Method. Kalman filter method has also been used to track the changing line parameters (14). The synchronized voltages and currents taken at the two terminals of the line at discrete time instants are used to estimate the line parameters. Based on Figure 3, we have

$$\begin{bmatrix} I_S \\ I_R \end{bmatrix} = \begin{bmatrix} V_S & V_R \\ V_R & V_S \end{bmatrix} \begin{bmatrix} a \\ b \end{bmatrix} \quad (37)$$

where the notation is the same as in the preceding section.

In Kalman filter method, we need to define the state, here as $x = \begin{bmatrix} a \\ b \end{bmatrix}$. Assume that N sets of measurements ($I_{S1}, I_{R1}, V_{S1}, V_{R1}, \dots, I_{SN}, I_{RN}, V_{SN}, V_{RN}$) are available. Then, the k th ($1 \leq k \leq N$) true state is denoted as $x_k = \begin{bmatrix} a_k \\ b_k \end{bmatrix}$. The following process is used to estimate the states:

The priori estimate \hat{x}_k^- at time k is treated as the same as the value at time $k-1$, because it is assumed that

the line parameter remains constant during a short time window

$$\hat{x}_k^- = \hat{x}_{k-1} \quad (38)$$

Then, the priori error covariance matrix \mathbf{P}_k^- is calculated as

$$\mathbf{P}_k^- = \mathbf{P}_{k-1} + \mathbf{Q} \quad (39)$$

where \mathbf{Q} is the process noise covariance matrix. The Kalman gain \mathbf{K}_k is acquired as

$$\mathbf{K}_k = \mathbf{P}_k^- \mathbf{H}_k^T (\mathbf{H}_k \mathbf{P}_k^- \mathbf{H}_k^T + R)^{-1} \quad (40)$$

$$\mathbf{H}_k = \begin{bmatrix} V_{p_k} & V_{q_k} \\ V_{q_k} & V_{p_k} \end{bmatrix} \quad (41)$$

where R is the observation noise covariance.

The posteriori estimate of the k th state is obtained as

$$\hat{x}_k = \hat{x}_k^- + \mathbf{K}_k (z_k - \mathbf{H}_k \hat{x}_k^-) \quad (42)$$

$$z_k = \begin{bmatrix} I_{p_k} \\ I_{q_k} \end{bmatrix} \quad (43)$$

The posteriori error covariance matrix \mathbf{P}_k needs to be updated as

$$\mathbf{P}_k = (\mathbf{I} - \mathbf{K}_k \mathbf{H}_k) \mathbf{P}_k^- \quad (44)$$

The value of \hat{x}_k after the k th iteration will give $\begin{bmatrix} \hat{a}_k \\ \hat{b}_k \end{bmatrix}$.

To enhance the tracking performance, an adjusted Kalman gain method may be used, where more weights are given to the given measurements to track the changing parameters faster. This method is essentially the same as the standard method, except that the posteriori estimate is calculated as

$$\hat{x}_k = \hat{x}_k^- + D\mathbf{K}_k (z_k - \mathbf{H}_k \hat{x}_k^-) \quad (45)$$

where $D > 1$ is the adjustment factor.

As to the parameter estimation accuracy, the least-squares and the Kalman filter methods are similarly accurate for estimating the static line parameters, and the Kalman filter method is more suitable to tracking dynamically changing line parameters. The parameter estimation accuracy is affected by the voltage and current measurement accuracy, and for a detailed discussion, the reader is referred to References 9 and 14.

These methods can be readily extended to unbalanced transmission lines, where parameters may be estimated using mode or phase equations.

5. FAULT LOCATION APPROACHES BASED ON THE USE OF FAULT TRANSIENTS

A solution of a linear partial differential equation may be found using the method of characteristics. The justification for this method may be found, for example, in Reference 15. The partial differential equations 1 and 2 of the transmission-line model have two characteristics: functions of position and time. The general solution for the voltage and current along the line is a linear combination of two arbitrary functions. Each function has one of the

characteristics as its argument. The particular value of these functions is set by the boundary conditions. The boundary conditions may be the measured voltage and current signal at the same point on the line. Two arbitrary functions are selected so that the general solution at this point equals the measured values.

Two approaches based on the partial differential equation model have been proposed for the fault location. The first method solves the partial differential equations using numerical methods with sending-end voltage and current as boundary conditions. An inspection of the voltage solution along the line reveals the fault location. The second method does not require the solution of partial differential equations, but instead it exploits a special property of the sending-end voltage and current and finds the distance by pertinent signal processing.

5.1. Partial Differential Equation-Based Methods

This method was first proposed by Kohlas for the case of the one-phase transmission line (16). Kohlas neglected the conductance in equation 2 to obtain a hyperbolic wave equation expressed in dimensionless (per unit) quantities as follows:

$$u_x(x, t) - x^2 i_t(x, t) = \eta i(x, t) \quad (46)$$

$$u_t(x, t) - i_x(x, t) = 0 \quad (47)$$

In these equations, $u = -cv(x, t)$, and $\eta = re$. This pair of equations has two characteristics: $t - x^2$ and $t + x^2$. These characteristics are the parallel lines in the position-time plane as given in Figure 4. The lengths along the two characteristics are denoted ρ and s , respectively.

Along a characteristic, functions u and i are related by the following two differential equations:

$$\begin{aligned} \frac{du}{ds} - x \frac{di}{ds} &= (1 + x^2)^{-0.5} \eta i \\ \frac{du}{dp} + x \frac{di}{dp} &= -(1 + x^2)^{0.5} \eta i \end{aligned} \quad (48)$$

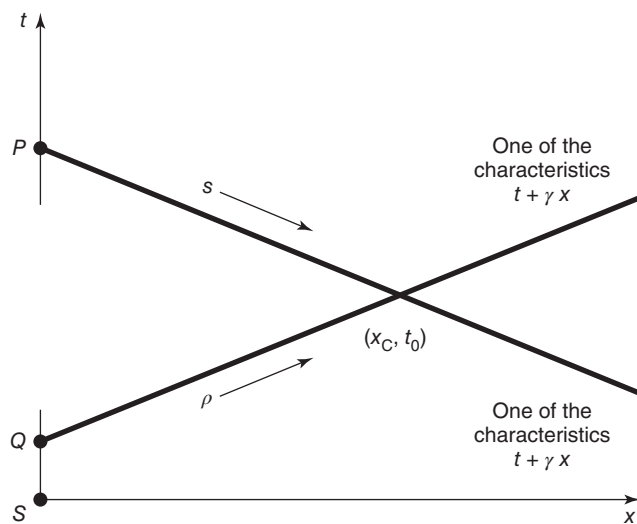


Figure 4. Characteristics in the dimensionless position-time plane.

These two equations may be solved numerically using the method of meshes described in Reference 15. The solution is obtained using the sending-end voltage and current as the boundary conditions. It is important to note that the value of the voltage does not depend on all the values of the sending end voltages and currents. The voltage depends only on the boundary conditions in just one segment of time. To find this segment, it is necessary to identify two characteristics passing through the point (x_0, t_0) (see Figure 4). These two characteristics intersect the t -axis at the two points P and Q . Only the values of t between these two points affect the value of $v(x_0, t_0)$. This time interval is called the zone of influence.

The fault location is found by an inspection of the voltage along the line using a property of the voltage. If the fault resistance is zero, as in Kohlas' paper, then the value of the voltage at the fault must be equal to zero. Accordingly, the location of the fault is equal to that value of x that annihilates the voltage at any time t . When the measurements contain noise, or when the fault impedance has a low but still nonzero value, one cannot expect the exact cancellation of the voltage $v(x, t)$ but rather a minimal value in some sense. Thus, when the solution for $v(x, t)$ is found, the next task is to look for the value of x at which the voltage is minimal. The problem here is that voltage depends both on the distance x and time t . Instead of inspecting the voltage as a function of time and distance, Kohlas proposed to inspect the function of distance $F(x)$ that is defined as the square of the voltage averaged in a specific time interval determined by the zone of influence:

$$F_{(x)} = \int_{yx}^{T-yx} v^2(x, t) dt \quad (49)$$

The value of x that minimizes the function $F(x)$ is the estimate of the distance to the fault. The Kohlas idea was subsequently extended and elaborated in detail for the three-phase transmission lines in Reference 17. In this reference, the three-phase transmission line is described by two matrix equations:

$$\mathbf{V}_x = \mathbf{L}\mathbf{I} + \mathbf{R}\mathbf{I} \quad (50)$$

$$\mathbf{I}_x = \mathbf{C}\mathbf{V}_x \quad (51)$$

where the subscripts x and t denote partial derivatives.

The matrices \mathbf{L} , \mathbf{C} , and \mathbf{R} have both diagonal and off-diagonal terms. Therefore, the preceding matrix equations cannot be solved using methods described by Kohlas. In addition, the elements of these matrices depend on the transmission-line geometry and copper resistance only if the ground is not used as a return. If the line is grounded, the matrices depend on the soil conductivity also. This parameter may depend on the weather and type of soil and cannot be easily determined. To complicate the matter further, as a repercussion, the line parameters then become frequency dependent. Fortunately, the two-matrix partial differential equations reduce to three pairs of decoupled partial differential equations similar in form to equation 15 by applying modal transformation as reported in Reference 17.

Modal transformation starts with finding three eigenvectors or the matrix product \mathbf{LC} . These vectors are columns of the transformation matrix \mathbf{M}_1 . The transpose of the matrix is \mathbf{M}_2 . The phasor voltages and currents \mathbf{V} and \mathbf{I} are transformed into modal voltages and currents $\mathbf{V}^{(m)}$ and $\mathbf{I}^{(m)}$ using the following equations:

$$\mathbf{V}^{(m)} = \mathbf{M}_1^{-1}\mathbf{V} \quad (52)$$

$$\mathbf{I}^{(m)} = \mathbf{M}_2^{-1}\mathbf{I} \quad (53)$$

The matrices \mathbf{R} , \mathbf{L} , and \mathbf{C} are also transformed to modal matrices $\mathbf{R}^{(m)}$, $\mathbf{L}^{(m)}$, and $\mathbf{C}^{(m)}$:

$$\begin{aligned} \mathbf{R}^{(m)} &= \mathbf{M}_1^{-1}\mathbf{R}\mathbf{M}_2 \\ \mathbf{L}^{(m)} &= \mathbf{M}_1^{-1}\mathbf{L}\mathbf{M}_2 \\ \mathbf{C}^{(m)} &= \mathbf{M}_1^{-1}\mathbf{C}\mathbf{M}_2 \end{aligned} \quad (54)$$

The particular feature of modal matrices is that their off-diagonal terms are equal to zero. Indeed, the modal transformation has the same advantage as the symmetrical component transformation. Actually, if a line is fully transposed, the symmetrical component transformation or the Clarke transformation will have the same decoupling outcome as the modal transformation. After the application of modal transformation, the transmission-line model consists of three decoupled pairs of linear partial differential equations:

$$\begin{aligned} \frac{\partial v_{kk}^{(m)}}{\partial x} + r_{kk}^{(m)} \frac{\partial i_{kk}^{(m)}}{\partial x} &= r_{kk}^{(m)} i_{kk}^{(m)} \\ c_{kk}^{(m)} \frac{\partial v_{kk}^{(m)}}{\partial t} - \frac{\partial i_{kk}^{(m)}}{\partial x} &= 0 \end{aligned} \quad (55)$$

Here, the subscript $k = 1, 2, 3$ denotes three modes, and x and t denote partial derivatives. One of the modes, known as the aerial mode, has parameters that are least dependent on frequency. Usually, only the aerial mode is considered for the fault location. Once a mode is selected, the procedure for the transmission-line model solution is the same as that for the one-phase transmission line.

5.2. Traveling-Wave-Based Methods

Traveling-wave methods do not require the solution of partial differential equations. In this approach, the line resistance r is neglected as is the line conductance c . Such a line is known as a lossless transmission line, and the describing equation is known as the telegrapher's equation. A simplification of this kind is appropriate for long and high-voltage transmission lines. The solution of the two equations then has a rather simple form. The voltage and the current are linear combinations of two components known as the forward and backward traveling waves and denoted S_F and S_B , respectively

$$v(x, t) = [S_F(t - x) + S_B(t - x)]/2 \quad (56)$$

$$i(x, t) = [S_F(t - x) + S_B(t - x)]/2Z_0 \quad (57)$$

where $Z_0 = \sqrt{l/c}$ is the surge impedance of the line and $\eta^2 = lc$.

The forward and backward traveling waves may be calculated from the sending-end voltage $v(0, t) = v_s(t)$ and the sending-end current $i(0, t) = i_s(t)$ as follows:

$$S_F(t) = v_s(t) + Z_0 i_s(t) \quad (58)$$

$$S_B(t) = v_s(t) - Z_0 i_s(t) \quad (59)$$

Fault location uses the transient component of the traveling waves only. The transient traveling waves appear in the transmission line after any abrupt change of its voltages and currents. When a fault occurs, the voltage at the fault point drops. This generates a backward and a forward traveling wave at the place of the fault. The backward wave travels to the sending end with a speed η^{-1} , and the forward wave moves to the receiving end with the same speed.

These traveling waves do not change their shape until they reach some discontinuity in the transmission line. The discontinuities are the sending end, the receiving end, and the fault itself. When a traveling wave arrives at a discontinuity, it ceases to exist in its original form, and two new waves emerge at the discontinuity. The first is reflection of the original wave; it has the shape of the original wave attenuated by a reflection coefficient, and it has a reverse direction. This reflection of the forward wave will be a backward wave. The second wave discussed here, *through wave*, also has the shape of the original wave attenuated by another coefficient and continues motion in the direction as the original wave. The coefficients affecting the magnitudes of new waves depend on the type of fault. Low impedance faults have high coefficients of reflection, and high impedance faults have low coefficients of reflection.

The motion of traveling waves along the transmission line and the generation of new waves at points of discontinuity are represented by the lattice diagram in Figure 5. The initial wave arises at the fault point F . The backward wave reaches the sending end at a time t_1 . Its reflection moves as a forward wave toward the fault. At the fault, it is reflected again and converted to a backward wave. It will arrive at the sending end at a time t_2 .

The time that elapses between the first reflection and the second reflection $\Delta t = t_2 - t_1$ depends on the distance to the fault x and the speed of travel:

$$\Delta t = 2Zx_x \quad (60)$$

The idea to use reflections to estimate the fault location appeared in 1930 for the fault location of underground cables. A cable is energized with a short-voltage impulse. The impulse and its reflection are recorded, and the travel time is found. Later, similar devices were used to measure the fault location for transmission lines. These methods are called active methods.

The calculation of the elapsed time is easy if the inserted pulse and its reflection have sufficient power. However, traveling waves caused by a fault may have a low lower power, especially if the fault occurs when the instantaneous voltage at the point of the fault is close to zero. In that case the calculation of this time requires special signal processing. One of the signal-processing methods most commonly used is the correlation technique (18).

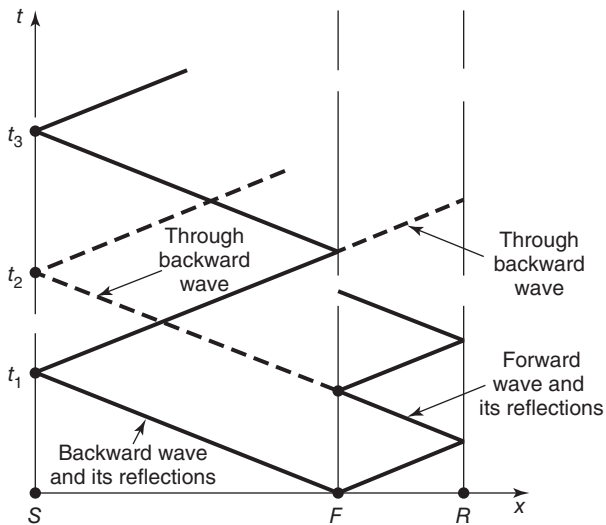


Figure 5. Lattice diagram.

The time autocorrelation of the signals $x(t)$ is defined as

$$R(\tau) = \lim_{T \rightarrow \infty} \frac{1}{2T} \int_{-T}^T x(t)x(t+\tau)dt \quad (61)$$

In real situations, the integration has to start and end within some finite time.

$$R(\tau) = \frac{1}{T} \int_0^T x(t)x(t+\tau)dt \quad (62)$$

For a given signal, autocorrelation is a function of the time shift T . Consider a typical shape of a traveling wave at the sending end, as shown in Figure 6a, and its time-shifted value shown in Figure 6b. The autocorrelation is proportional to the area of the product of two signals. This area will be largest when the first reflection is aligned with the second reflection as in Figure 6c. Then, the time shift is equal to the elapsed time $t_2 - t_1$. Therefore, the elapsed time may be assessed by investigating the maxima of the autocorrelation function.

In fault location algorithms, the digital version of the autocorrelation function $\vartheta(k)$ is calculated using the frequency f and denoted here as $x(i)$:

$$\vartheta(k) = \sum_{i=1}^N x(i)x(i-k) \quad (63)$$

The accuracy of the fault location is very sensitive to the choice of T and N . If T is too small, the approximation is not good since an important part of the signal may be missing. On the other hand, if T is too large, the shape of the forward wave will contain multiple reflections of both the original backward and the original forward waves. For example, such a reflection will appear at time t_3 in the lattice diagram. Also, in nonsymmetrical faults, a fraction of a traveling wave in one mode may appear in another mode. As a result, the autocorrelation will have more maxima, and the identification of the maxima corresponding to the first reflection and second reflection will be difficult. In general, the closer the fault to the sending end, the shorter the window is needed. The other important factor is the sampling

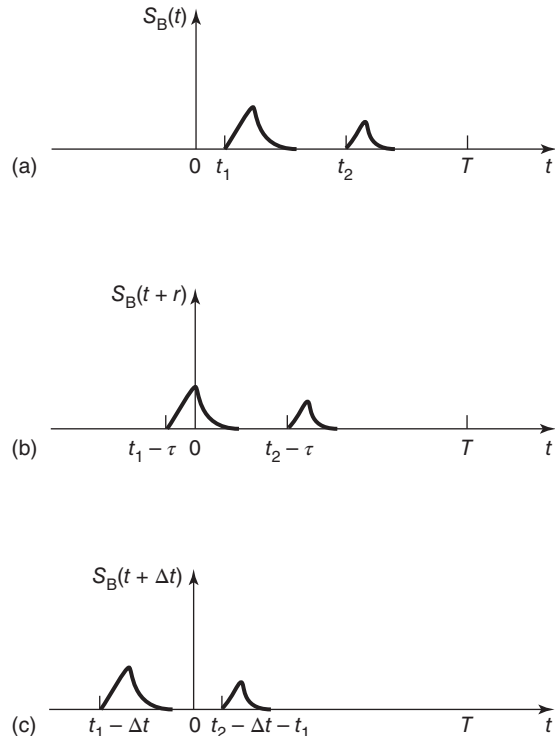


Figure 6. (a) Typical backward wave. (b) Shifted backward wave. (c) The product of $S_B(t)$ and $S_B(t+r)$ is maximum when $r = \Delta t$ and the second and first reflections are aligned.

frequency. In general, a very high sampling frequency (on the order of tens of kilohertz) is needed to ensure a good approximation of the autocorrelation function.

The limitations of this approach are (i) a lack of firm rules in the selection of the sample window due to its sensitivity to the fault distance, (ii) the possibility of obtaining a false result due to the presence of multiple reflections, and (iii) a high sampling frequency, increasing the computational burden.

6. FAULT LOCATION USING SHORT-CIRCUIT MODELS

Every protection engineering department – from the smallest municipal utility to large investor-owned utilities – uses a short-circuit software program (PSS[®]CAPE, ASPEN OneLiner, SKM Power Tools, ETAP, etc.) to model its power system. While the calculation of protective relay settings and testing of protective relay selectivity and sensitivity is the principal application of the short-circuit model, it is also used for other purposes such as circuit breaker rating studies, postmortem analysis of system events triggered by protection operation, and fault location.

In this section, we explore the use of a typical short-circuit model in locating transmission system faults. The techniques presented in this article span the range from simple, manual methods that utilize phasor-based oscillography from measurement devices in the power system to more complex, automated techniques that are able to

process measured time-domain voltage and current information in an attempt to locate the fault.

Such methods are usually offline in nature – that is, the oscillography or other measurement data must be provided to the engineer for subsequent processing within the short-circuit model. The use of short-circuit models in real-time location of faults and validation of protection operation is a natural extension, and several industrial applications are available that facilitate this.

6.1. Short-Circuit Model Characteristics and Limitations

The short-circuit models used by protection engineers are based on a sequence representation of the electrical network. Such a representation implicitly assumes that the default state of the network is balanced, and that any unbalance is introduced as a result of a short-circuit fault or other change such as a breaking of a single conductor and opening of a single pole in a circuit breaker (19).

The sequence representation also necessitates assumptions to be made on the modeling of the individual components that make up the power system. These assumptions are:

- Synchronous generators are assumed to be ideal voltage sources, behind a constant source impedance. A similar representation is used for synchronous and induction motors, although their contribution to short-circuit conditions lasts for only a few cycles after the fault, unlike that of generators. In some short-circuit programs, the varying nature of the impedance of a synchronous generator is accounted for when studying sequential fault clearing scenarios.
- Inverter-based resources are typically accounted for as ideal current sources or voltage-dependent current sources – that is, there is no source impedance associated with such devices.
- Transmission lines are modeled using the lumped-parameter $R + jX$ representation; this implies full transposition of the line, without any mutual coupling between the individual phases.
- When transmission lines exist in the same right of way, coupling between the lines is assumed to exist only in the zero sequence; coupling in the positive and negative sequences is ignored.
- Transformers are also modeled using lumped parameters, with a positive-sequence impedance and a zero-sequence impedance depending on the transformer winding type, grounding, etc. Negative-sequence impedance is assumed to be the same as the positive-sequence impedance.
- Capacitors, inductors, loads, switched capacitor banks, and line-charging capacitance are also included in the short-circuit model.
- The behavior of nonlinear devices such as metal oxide varistors (MOVs) used for the protection of series capacitors is approximated using iterative methods.

With these assumptions, the calculation of a short-circuit fault and the subsequent current distribution in the power system model take place as follows:

1. Solve a power flow in the network to establish a voltage magnitude and angle at every node in the system. This also results in the so-called prefault current flow in the network.
2. At the location of the fault, develop the Thevenin impedance of the network using the bus admittance matrix Y_{BUS} .
3. Calculate the fault current as the ratio of the prefault voltage at the fault location and the Thevenin impedance. This fault current will redistribute itself in the network branches and also set up the postfault voltage at each network node. See equation 64.

$$I_{\text{Fault}} = \frac{V_{\text{Prefault}}}{Z_{\text{Thevenin}}} \quad (64)$$

4. In each network branch, calculate the final current as the vector sum of the prefault current flow and the fault current flow. Such a vector sum is possible since we assume that the power system is a linear network.

Protective relays respond to the final currents that flow in the branches they are applied on and the postfault voltages at the bus where they are connected.

While the use of the short-circuit model and attendant fault calculations is very effective in determining settings for protective relays, its success in locating faults accurately can vary, depending on the following:

- The accuracy of the impedance data used for the generators, lines, transformers, etc., that is, the accuracy of the short-circuit model.
- The accuracy with which the state of the system in terms of actual generation in use, status of circuit breakers and switches, actual system loading, etc. is replicated in the short-circuit model.
- The use of phasor-based models of various power system equipment, which ignores the transient nature of faults, adds to the uncertainty of fault location using short-circuit models.

Still, short-circuit models are useful in providing a quick estimate of the location and help guide a repair crew to the general vicinity of the fault.

6.2. The Basic Fault Location Techniques Utilizing Short-Circuit Program

The basic fault location techniques use oscillography data such as current magnitude, faulted phase, and faulted line captured from devices such as relays and disturbance fault recorders (DFRs). These data are provided to the short-circuit program, which moves the fault location (manually or in an automated manner) to match the fault current produced by the model with the oscillography (20).

Fault Location Using Measurement from One Terminal Utilizing Short-Circuit Program. This method tries to locate the fault on a line, using measurements from one terminal of the faulted line or some other line in the vicinity. The inputs provided by the user are as follows:

- Status of the remote-end breaker of the faulted line at the time of the measurement.
- The line on which the fault occurred.
- Fault type.
- The line terminal where the measurement (current) was recorded; this need not be the same as the faulted line.
- The phase of the monitored current – I_A , I_B , I_C , or neutral ($3I_0$).
- Magnitude of the monitored current.
- If additional measurements are available, the user will have the opportunity to enter those to help refine the fault location.

This approach requires the knowledge of the faulted line, fault type, and the status of the remote-end breaker – such information can be gleaned from the oscillography and other DFR or relay data. It is also important to match the initial state of the short-circuit model with the actual system configuration. This can be harder to achieve, unless there is a way to import SCADA data directly into the model.

Once the data have been provided, the fault locator will perform an iterative search on the faulted line and repeatedly apply faults on the line, while comparing the model's output with the measured current. When the difference between the calculated current and the measured current reduces to a certain threshold, that particular location is identified as the actual fault location and reported to the user.

An example from a commercial short-circuit program is shown below. The measured current is 1549 A (primary), and the fault is known to have occurred on a transmission line between buses A and B. It is also known to be a three-phase fault. Measurement is at Bus A.

FAULT LOCATOR W/CLOSED FAR END BREAKER:

1549 Pri. A

Searching for location of a solid fault with given line-end current

Faulted Line

Local end: From BUS A To BUS B Ckt 1

Remote end: From BUS B To BUS A Ckt 1

Fault Type: A-B-C

Fault recorder information

Location: From BUS A To BUS C Ckt 1

Specified Current: 1549.0 Amps (Ia)

Calculated currents

Local Bus Fault: 2567.3 Amps

Remote Bus Fault: 1426.9 Amps

Actual Current: 1553.4 Amps

Error: -4.4 Amps

Total No. of Iterations: 5

Fault location: 84.31% From BUS A to BUS B

The iterative application of a three-phase fault on the line results in the fault being located at 84.31% from Bus A. This percentage is based on the positive-sequence impedance of the line and can be translated to the appropriate distance in km or miles. Note that it took five

iterations for the difference between the calculated current and measured current to reduce below the threshold.

In the event that the iterative approach is not able to locate the fault between 0% and 100% of the line impedance, a suitable warning is provided. An example from a commercial short-circuit program is shown below. The fault is on a line from Bus A to Bus B. The measured current is 3500 A (primary), at Bus A. However, according to the short-circuit model, there is no location on the line for which the short-circuit faults produce 3500 A at Bus A.

Faulted Line

Local end: From BUS A To BUS B Ckt 1

Remote end: From BUS B To BUS A Ckt 1

Fault Type: A-B-C

Fault recorder information

Location: From BUS A To BUS C Ckt 1

Specified Current: 3500.0 Amps (Ia)

Bad Run (CURRENT SPECIFIED IS TOO > HIGH < TO LOCATE FAULT ON SUSPECTED LINE)

This example highlights one of the limitations of the model-based fault location approach. It is possible that a certain combination of generation and circuit breaker configuration, not accounted for in the model, may result in a fault location on the line that produces 3500 A at Bus A. If such network information were available, the model can be updated prior to applying the fault location.

Fault Location Using Measurements from All Terminals Utilizing Short-Circuit Program. A variation of the single-ended fault locator utilizes measurements from all terminals of the faulted line. Unlike the single-ended fault locator, however, measurements from the nonfaulted line cannot be processed by the multiended fault locator. At the same time, knowledge of the fault type and faulted phase is necessary. A by-product of the multiended fault locator is that it produces an estimate of the fault impedance as well, if justified by the measurements.

In the example below (from a commercial short-circuit program), the fault locator is provided with two measurements: 1800 A from the local terminal (Bus A) and 4430 A from the remote terminal (Bus B). The fault location was determined to be 52.83% from the local terminal (in terms of line impedance), with a fault resistance of 0.68 Ω .

Faulted Line

Local end: From BUS A To BUS B Ckt 1

Remote end: From BUS B To BUS A Ckt 1

Fault recorder information

Fault Type: THREE PHASE Current Type: Phase

Local end current (A): 1800

Remote end current (A): 4430

Fault location: 52.83% From BUS A To BUS B

Fault Resistance (Ohms): 0.68

Determining Fault Resistance Using Short-Circuit Program.

For postmortem analysis, the resistance of a fault that occurred in the system may be of interest to the engineer. With the knowledge of the fault type, fault location, and at least one measurement from the faulted line or elsewhere, the resistance of the fault can be determined. This information can be used to recreate the actual fault scenario in the short-circuit model and test whether protective relays operated as expected.

In the example below (from a commercial short-circuit program), the fault location (52.53%), fault type (three-phase fault), and measured current (1800 A at Bus A) are provided as inputs to the calculation. The algorithm determines the fault resistance to be 0.74 Ω.

Calculation of Arc Resistance from Measured Current and Fault Location

Fault Location

52.53% From BUS A To BUS B Ckt 1

Fault recorder information:

Fault Type: THREE_PHASE Current Type: Phase

Location: From BUS A To BUS C Ckt 1

Monitored current (A): 1800

Fault arc resistance 0.74 ohms

6.3. Advanced Fault Location Techniques Using DFR Measurements Utilizing Short-Circuit Program

DFR measurements are typically made available as COMTRADE files with time-domain voltage and current information. These data can be processed and converted to phasors, followed by the analysis using standard single- and double-ended fault location algorithms available in the literature (21):

1. Single-ended reactance method based on the compensated apparent impedance. Ignores the fault resistance.
2. Single-ended reactance method based on the loop impedance, valid only for a radial line ($I_A = 3I_0$).
3. Single-ended Takagi method with polarization by the faulted phase current.
4. Single-ended Takagi method with polarization by the measured I_0 current.
5. Single-ended modified Takagi method with accurate knowledge of the state of the network prior to the fault.
6. Two-terminal negative sequence.
7. Two-terminal Takagi with the total fault current measured.

Since the fault location algorithms depend on the calculation of voltage and current phasors, the fault location estimates take some time to settle down, while the phasor estimates settle to a final value. The Takagi and Reactance Radial algorithms typically produce fault location estimates that are consistent with each other.

The single-ended modified Takagi method utilizes the source impedance behind the measurement location to

determine the location of the fault. Therefore, it is important to update the short-circuit model with the correct generation levels and topology state *prior* to fault location.

6.4. Automated Fault Location and Analysis

The methods described in Section 6.2 are offline techniques – oscillographic data or DFR measurements are downloaded and provided to an engineer who performs the analysis and returns the results to the appropriate utility group for further action. In recent years, considerable R&D effort has been expended in automating the fault location and analysis process, so that the availability of an engineer to run the studies does not impact the immediate availability of the results.

Also, helping the automation is the fact that SCADA data, short-circuit network model data, protective relay settings information, and protection simulation programs are all accessible via company-wide intranets. Therefore, the moment oscillographic data or DFR data become available, fault location and event analysis can be automatically triggered in the following steps:

1. Superimpose the SCADA data on the base network model to update it
2. Download the DFR, relay, or other oscillographic data
3. Apply suitable fault location algorithms to determine the fault location
4. Recreate the event by simulating protective relay behavior in the model
5. Determine if relay behavior is appropriate and matches the actual relay behavior
6. Generate suitable reports and disseminate for further action

Several commercially available tools are able to perform one or more of the activities listed above, and their proliferation is expected to continue in the future.

7. FAULT LOCATION USING ELECTROMECHANICAL OSCILLATIONS

In recent decades, development of phasor measurement units (PMUs) introduced various synchrophasor-based fault location methods (22–25). In References 22 and 23, Clarke transformation is applied to the synchronized voltage and current phasors aligned with a discrete Fourier transform-based algorithm to calculate the location of fault. Another fault detection/location technique is presented in References 24 and 25 with consideration of arcing fault discrimination based on synchronized fundamental phasor measurements. In Reference 26, a bus-impedance matrix was utilized to calculate the fault point with access to limited synchronized measurements at two remote buses in the network. Several methods utilize electromagnetic transient propagation in power system and are known as traveling wave-based methods (27–31). The method proposed in References 27 and 28 is based on measuring the time of arrival (ToA) of electromagnetic traveling waves which propagate from the

fault point to sparsely located synchronized measurement devices. Then, an optimization method is applied to calculate the location of fault. In Reference 29, a wide area traveling wave-based method is proposed, which determines faulty line and distance to fault by analyzing the traveling wave propagation times using the extended double-end method. In Reference 30, a traveling wave principle along with two graph theory-based lemmas is deployed to sectionalize power system and locate faults within the suspected sections. Despite the high accuracy of the traveling wave-based methods, they require a measurement device with high sampling rate to capture the electromagnetic transient, which increases the cost of implementation.

The method discussed in this article is based on the detection of ToA of electromechanical-wave oscillation propagates in power system. Unlike the electromagnetic traveling wave-based methods, the proposed method relies on sparse PMU measurements and can be practically used by utilities without requiring expensive dedicated high sampling rate devices.

7.1. Background Theory

Electromechanical Wave Propagation Phenomena. When a disturbance occurs on a transmission line, the electrical power flow changes in the network. This leads to a mismatch between the electrical and the mechanical torque of generators located in the vicinity. Therefore, each generator rotor angle changes to compensate the mismatch. Following the generators' rotor angle oscillations, the adjacent buses also encounter changes in their generators' rotor angle, which again causes a mismatch in the electrical torque of the adjacent generators. In this fashion, the oscillation known as the electromechanical-wave propagation is "seen" throughout the entire network. Electromechanical oscillations could be detected by monitoring the phasor angle of bus voltages and characterized with much lower frequency (0.1–10.0 Hz) than the electromagnetic transients (>100 kHz) (31). To illustrate the concept, a simple power-system model in the form of a ring is used. Figure 7a shows the 64-generator ring system, which comprises 64 identical serially connected generators through identical transmission lines, forming a ring. The initial bus angles are evenly distributed from 0 to 360° by steps equal to $360^\circ/64 = 5.625^\circ$. Due to homogeneity and the ring shape of the 64-bus system, it is well suited to study the basic aspects of the electromechanical-wave propagation phenomena. Figure 7b shows the phasor angle of 64 buses (in radian) with respect to time of a given disturbance occurring at bus 16 at $t = 0$. Following the change in the angle of bus 16 shown by the red line in Figure 7b, the other generators react in a similar fashion, but with a certain time delay. Plotting all the bus angles together, this time delay can be represented as a wave modulated on the phasor angles of the buses, which travels away from the disturbance source into the network at a finite speed.

Continuum Modeling. Applying differential algebraic equations (DAEs) is the conventional way of modeling electromechanical-wave propagation in power system.

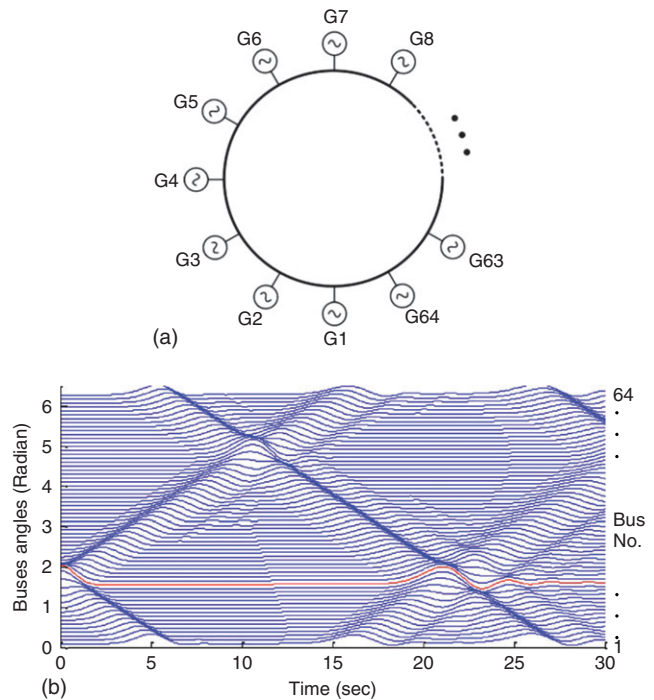


Figure 7. Understanding electromechanical-wave propagation. (a) 64-generator ring system. (b) Bus angle modulation following a fault at bus 16 at $t = 0$.

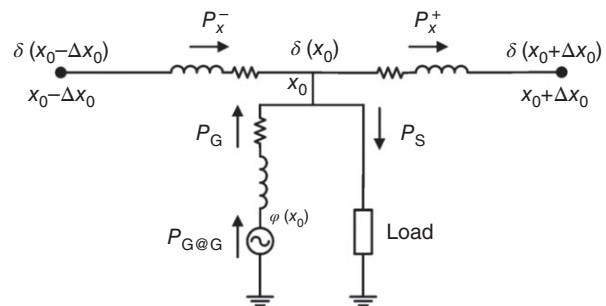


Figure 8. Incremental system used for continuum modeling of system at x_0 .

Due to complexity, this approach could be time consuming, and the result would be hard to analyze for large networks. Therefore, researchers introduced a much simpler method which embeds the effect of electromechanical wave propagation into power system behavior (31–35). The so-called continuum model considers power system with spatially distributed parameters. The continuum model is based on applying partial differential equations (PDEs) describing the power systems to the infinitesimal element distributed along the power system. Due to the generators rotor inertia, the timescale of electromechanical oscillations is large compared to the power system frequency. Therefore, the variables in continuum model can be considered as phasor parameters (35). In the context of continuum modeling, any point in the power system could be represented by the incremental system as shown in Figure 8.

The model allows for representation of lines with different per-unit impedances, shunt reactances, generators, and loads. The flexibility of the incremental model allows any arbitrary network topology to be modeled with continuum approach. Following is a summary of the continuum formulation.

In Figure 8, the net real electrical power flow at point can be written as equation 65

$$P = \frac{R}{\Delta x |Z|^2} [1 - \cos(\delta(x_0) - \delta(x_0 \pm \Delta x))] + \frac{X}{\Delta x |Z|^2} \sin(\delta(x_0) - \delta(x_0 \pm \Delta x)) \quad (65)$$

where $\delta(x)$ represents the phase angle of voltage at x , and R , X , and Z represent the resistance, reactance, and impedance of the branch, respectively. Using Taylor series expansion about x_0 and disregarding higher order terms, we get

$$P = \frac{R}{|Z|^2} \left(\frac{\partial \delta(x_0)}{\partial x} \right)^2 \Delta x - \frac{X}{|Z|^2} \left(\frac{\partial^2 \delta(x_0)}{\partial x^2} \right) \Delta x \quad (66)$$

The real power produced at the generator terminal is determined by equation 67, and the real power delivered to the point x_0 by the generator is given by equation 68

$$P_{G@G}(x_0) = \Delta x G_{\text{int}} [1 - \cos(\delta(x_0) - \varphi(x_0))] + \Delta x B_{\text{int}} \sin(\delta(x_0) - \varphi(x_0)) \quad (67)$$

$$P_G(x_0) = \Delta x G_{\text{int}} [\cos(\delta(x_0) - \varphi(x_0)) - 1] - \Delta x B_{\text{int}} \sin(\delta(x_0) - \varphi(x_0)) \quad (68)$$

where G_{int} and B_{int} represent the conductance and susceptance of a generator. By conservation of power, the summation of power at a region must be zero, which implies

$$P = P_G - P_s \quad (69)$$

where P is the net real power flow at x_0 , P_G is the real power delivered by the generator, and P_s is the real power consumed by the load. Plugging equations 66, 67, and 68 into equation 69, we obtain

$$G \left(\frac{\partial \delta(x_0)}{\partial x} \right)^2 - B \frac{\partial^2 \delta(x_0)}{\partial x^2} = G_{\text{int}} [\cos(\delta(x_0) - \varphi(x_0)) - 1] - B_{\text{int}} \sin(\delta(x_0) - \varphi(x_0)) - G_s \quad (70)$$

which is known as the continuum equivalent of load flow equations of the power system. On the other hand, the internal generator phase angle dynamics are modeled using

$$m(x_0) \frac{\partial^2 \varphi(x_0, t)}{\partial t^2} + d(x_0) \frac{\partial \varphi(x_0, t)}{\partial t} = P_m(x_0) - \frac{P_{G@G}(x_0)}{\Delta x} \quad (71)$$

where $m(x_0)$ and $d(x_0)$ are the generator inertia and damping constant, and $P_m(x_0)$ is the mechanical power of a generator. Plugging equation 67 into equation 71, we obtain equation 72

$$m(x_0) \frac{\partial^2 \varphi(x_0, t)}{\partial t^2} + d(x_0) \frac{\partial \varphi(x_0, t)}{\partial t} = P_m(x_0) + B_{\text{int}} \sin(\delta(x_0) - \varphi(x_0)) - G_{\text{int}} [1 - \cos(\delta(x_0) - \varphi(x_0))] \quad (72)$$

which is known as the continuum equivalent of swing equations of the power system.

7.2. Methodology

As mentioned earlier, electromechanical wave originated following a disturbance travels with finite velocity in a given network. Since these waves propagate through different paths, they reach remote buses with distinct time delays, which depend on each path length and propagation speed of wave through that path. Therefore, one can determine the fault location using ToA measurements at various locations along with the supporting information to determine each path's length and speed of propagation through that path. The method discussed in this article detects ToA of electromechanical waves modulated on the phasor angle of voltage at selected buses where PMUs are available and then deploys Dijkstra's shortest path algorithm (36) combined with several mathematical steps to detect the faulty line. Finally, the location of the fault will be determined inside faulty line using binary search method. Details of the methodology are explained next.

Time of Arrival and Fault Type Detection. Leveraging supervised learning to analyze the first swing of the phasor angle obtained from PMUs, the ToA of electromechanical wave can be obtained. To differentiate between faults and other disturbances as well as different types of faults, three types of input signals are defined in the input layer. The phase angles of each three-phase voltages as well as their first- and second-time derivatives were selected as inputs. The inputs and the desired outputs are compared in a hidden layer, and errors are then propagated back through the system. Since the nature of the electromechanical-wave oscillation propagation and its related phase angle modulation is same for different networks, the ToA detector can be used for any given network.

Faulty Line Detection. Once the ToA of electromechanical-wave oscillation is obtained at selected buses where PMUs are installed, it can be used to determine the faulty line. Several mathematic steps as described below must be deployed before the faulty line could be detected.

(1) Computation of Line Propagation Delay

Based on continuum model, the speed of electromechanical-wave propagation through any network solely depends on the system parameters and can be obtained as follows (31):

$$v = \sqrt{\frac{\omega \sin \theta}{2h|z|}} \quad (73)$$

where ω is the nominal system frequency, θ is the line impedance angle ($\sim 90^\circ$), h is the inertia constant of generator, and $|z|$ is the line impedance. Therefore, the propagation delay of each line in the network can be calculated by

$$T_{\text{delay-L}} = \frac{x_L}{\sqrt{\frac{\omega \sin \theta}{2h|z|}}} \quad (74)$$

where $L = 1, \dots, l$ represents each transmission line in the network, and x_L is the total length of line L . So, if length and impedance of transmission lines are known,

electromechanical-wave propagation delay through each transmission line can be calculated using equation 74.

(2) Calculation of Measured ToA Matrix

Figure 9 is used to explain the computation of the shortest time-delay matrix. As shown in Figure 9, for the given network assume that PMU measurements are available at buses A, B, C, and D, while a fault occurs at an unknown bus k (this assumption will be removed later). The propagation delay of the electromechanical wave to reach bus A after fault occurs at bus k can be obtained by

$$t_{Ak} = t_A - t_k \quad (75)$$

where t_k represents the fault initiation time at bus k, t_A represents the ToA of electromechanical wave at bus A, and t_{Ak} is the propagation delay of the electromechanical wave to arrive at bus A. Since the fault initiation time t_k is unknown, it is impossible to obtain t_{Ak} . Suppose that bus A is the first to receive the propagated wave. It can be used as the time reference. Therefore, the wave propagation delay from bus k to bus B with respect to the ToA of the electromechanical wave at bus A (t_A) can be defined as

$$t_{BA} = t_{Bk} - t_{Ak} = (t_B - t_k) - (t_A - t_k) = t_B - t_A \quad (76)$$

It should be noted that equation 76 is always correct, since the electromechanical waves propagate along the transmission lines always following the shortest path rule. The electromechanical-wave propagation delay from bus k to other buses with respect to the ToA of the electromechanical wave at bus A (t_A) can be defined similar to equation 76. Hence, the measured propagation time-delay matrix can be defined as

$$T_{\text{meas}} = [t_{BA} \ t_{CA} \ t_{DA}] \quad (77)$$

(3) Calculation of Theoretical Time-Delay Matrix

Since the propagation delay of each transmission line is known by equation 74, the vector of time differences resulting from the shortest propagation delay could be computed as follows.

$$T_{\text{sp-x}} = [\tau_{Bx} - \tau_{Ax} \ \tau_{Cx} - \tau_{Ax} \ \tau_{Dx} - \tau_{Ax}] \quad (78)$$

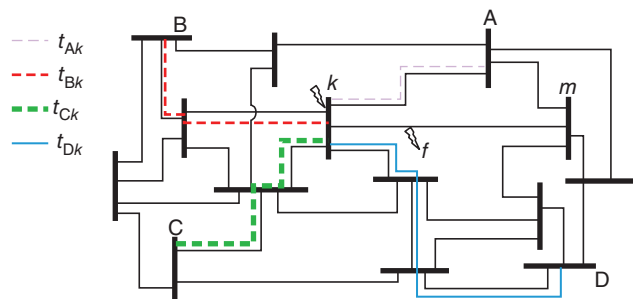


Figure 9. Illustration of the calculation of theoretical and measured delay matrices.

where τ_{Ax} , τ_{Bx} , τ_{Cx} , and τ_{Dx} are the theoretical shortest propagation time delay from buses A, B, C, and D to any arbitrary bus x, respectively. It can be rewritten as

$$T_{\text{sp-x}} = [\tau_{BAx} \ \tau_{CAx} \ \tau_{DAx}] \quad (79)$$

The shortest time-delay path for each bus pair is computed utilizing the Dijkstra's algorithm. One-time computation of equation 79 with Dijkstra's algorithm is valid for a given topology before any line switching takes place. After any topology changes, the calculation must be repeated to update the matrix elements.

(4) Definition of Minimum Error Function

As shown in Figure 9, if the fault occurs at unknown bus k, the calculated $T_{\text{sp-k}}$ should identically match the T_{meas} captured by ToA detectors. Therefore, one can define P_x as follows and then check it for all buses to find the bus that corresponds to the minimum (zero) value.

$$P_x = \text{Min}(\|T_{\text{sp-x}} - T_{\text{meas}}\|) \quad x = 1, \dots, n \quad (80)$$

where $x = 1, \dots, n$ is the total number of buses, and P_x is the minimum norm linked with bus x.

As stated before, we assume that faults only take place at buses, which is not realistic in actual power system. Consequently, the methodology must be revised, so that the method can be applied for any arbitrary fault located along the transmission lines. As shown in Figure 9, if the fault occurs at an arbitrary point f, two buses corresponding to the minimum two values obtained from equation 80 will be selected. The network topology will be checked to see if this pair of buses has a direct link to each other. If so, the line connecting these two buses will be declared as faulty line. If there is no direct link between the two buses, then each line connected to the two buses will be considered as the faulty-line candidate. Hence, fault location calculation must be repeated for all possible candidates, which can be tolerated due to limited number of lines connected to the pair of suspect buses.

Locating Fault Using Binary Search. Once the faulty line is determined, the exact location of fault can be derived by adding fictitious buses and dividing the faulty line into two-line segments (binary search approach (37)). As shown in Figure 10, the first fictitious bus divides the faulty line (mk) into two equal sections (a_1m and a_1k). Then, equation 80 will be recalculated for $x = a_1, m$, and k . Then, the two buses that correspond to the lowest P_x values will be treated as the faulty section. Similarly,

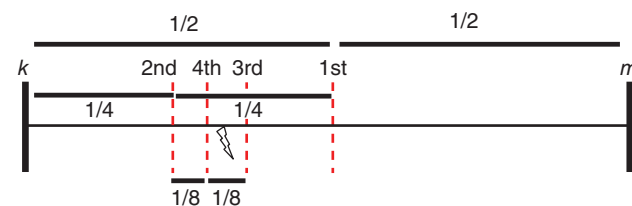


Figure 10. Illustration of the binary search used for fault location method.

the second fictitious bus divides the faulty section (a_1k in Figure 10) into equal sections (a_1k and a_2k) and so on. If this process occurs over and over, mathematically, after adding the i th fictitious bus, the location of fault will be determined within the following error:

$$E = \left(\frac{1}{2^i} \right) \times 100$$

7.3. Discussion on Accuracy and Trade-Offs

The proposed fault location methodology based on propagation of electromechanical-wave oscillation has been rigorously tested against different fault types, locations, system topology changes, and PMU bad data, and the summary is concluded as below:

- Unlike different wide area measurement-based methods that require information from all buses, the proposed method uses measurements from sparsely located PMUs, which reduce the cost of implementation.
- The calculation burden is less than most of the single- or multiple-end fault location methods, since the precalculated shortest path database using Dijkstra's algorithm will remain valid until the topology of the power system changes.
- The proposed method could be implemented with PMUs or any other IED devices, which can measure and report GPS synchronized phasors.
- The fault location error remains under 1% for all fault types and locations.
- The effect of PMU bad data is felt when the affected PMUs are less than two buses away from the faulty line.
- The accuracy of the methodology deteriorates once the topology of the system changes. The impact on accuracy remains negligible if the topology changes are more than two buses away from the faulty line.

8. FAULT LOCATION IN DISTRIBUTION SYSTEMS

Accurate fault location identification is one of the key functions for distribution management system programs. Once the location of the fault is identified, post fault-restoration process is carried out. A variety of fault location methods have been proposed as discussed in the following sections.

8.1. Summary of Methods

Impedance-Based Method. In this method, the apparent impedance between the fault location and the substation is estimated using the voltage and current phasor measurements. Once the total impedance is determined, the distance of the fault from the substation can be calculated since the per-length impedance values of the lines are available. The calculations can be performed in the sequence domain using zero, positive, and negative sequence components of the network (38) or in the three-phase domain (39).

Superimposed Method. This approach pinpoints the fault by finding the fault location that minimizes the superimposed values of the voltage and current in the healthy phases. The superimposed values are calculated by subtracting the pre-fault measured values from the during-fault measured values.

Traveling Wave Method. This approach is based on the traveling waves generated by the faults (40). The measurements can be performed at one end of the line or at both ends of the line at a sampling rate of 1–10 MHz. This method is more suitable for transmission lines as in the distribution systems the presence of laterals and sublaterals causes multiple reflections that make the task of detecting the arrival time of the traveling waves challenging.

Artificial Intelligence-Based Method. This method utilizes artificial intelligent methods for finding the fault locations (41). Features such as amplitude of the voltage and current measurements and patterns of change in the current and voltage amplitudes due to the operation of protective devices and reclosers are used for the training purpose. The drawback of this method is the fact that large number of training data are needed, and subsequent to the changes in the system topology, the patterns may change, which necessitates retraining of the algorithms.

Voltage Sag Data-Based Method. This approach is based on the comparison between simulated and measured signals (42). Faults at different locations are simulated, and the results are compared with the measured data from the power distribution systems. The fault scenario that generates signals with highest similarity with the measured data is the actual fault location. Advantage of this method is that it can be used for different types of distribution systems with different load types. However, it requires simulating many fault scenarios, which increases the computational burden of the method. Therefore, in Reference 43, a hybrid method has been proposed to reduce the computational burden of the method.

Micro-PMU-Based Method. In this method, synchronized measurements from Micro-PMUs are used for the fault location identification purpose. The advantage of using synchronized measurements is that in addition to the amplitude, the phase angles of the measured signals can be used for the fault location identification. For example, in Reference 44, a method using Micro-PMU data is proposed that operates based on the superimposed values of the measurements. This method requires the installation of Micro-PMUs.

8.2. Eliminating Multiple Fault Location Estimates

Fault location identification methods may estimate more than one location for the fault. In this case, the fault location method determines multiple fault locations that their electrical distances from the substation are the same as that of the actual fault location. Several methods

have been proposed to eliminate the false fault location estimations.

In Reference 38, data from fault indicators (FIs) are used to eliminate false estimates. However, possible loss of data and misoperations are not considered. In Reference 43, a method based on fuzzy Petri nets is proposed that utilizes collected status data such as the status of the protective devices and FIs and outage notifications from smart meters to eliminate false estimates. In this approach, in the first stage, the faulted zone is identified, and then, the voltage sag data-based fault location method is used to pinpoint the fault location. The advantage of this approach is that not only the problem of the multiple false estimations is solved but also the fault location estimation processing time reduces significantly as in the first stage the search space of the voltage sag data-based fault location method is significantly reduced, leading to a faster fault location identification.

In Reference 45, data collected from few meters along the feeder is utilized for eliminating the false estimates. Once the impedance-based fault location method identifies a short list of possible fault locations, faults at the identified locations are simulated, and the fault case that generates voltage and current values with highest similarity with the measured current and voltage values at the meter locations is identified as the actual location of the fault. To minimize the number of required meters, the problem of meter placement is formulated as a mixed-integer linear programming problem. The MILP-based method determines the minimum number of meters and the locations that they should be installed to assure that faults at different locations can be differentiated from each other.

In Reference 39 also, a method to eliminate the false estimations using the observed pattern of the operation of protective devices such as fuses and reclosers is proposed. The fault scenario that generates a similar pattern to the observed pattern of protective devices operation is identified as the actual location of the fault.

To further explain the procedure of the fault location identification in distribution systems, the procedure of a hybrid fault location method is discussed in this section. More details of this method are presented in Reference 45.

First, a short list of possible fault locations is identified using an impedance-based fault location method. The impedance-based fault location method determines all possible fault locations that are at the same electrical distance from the substation. To eliminate the false estimates, in Reference 45, a voltage sag-based fault location is utilized. Fault scenarios are simulated by applying faults at the identified possible fault locations. To estimate the fault resistance, the procedure shown in Figure 11 is used in which

$$\varepsilon = |I_{\text{simulated}}| - |I_{\text{recorded}}| \quad (81)$$

where

$|I_{\text{simulated}}|$ is the amplitude of the simulated current phasor at the substation.

$|I_{\text{recorded}}|$ is the amplitude of the recorded current phasor at the substation.

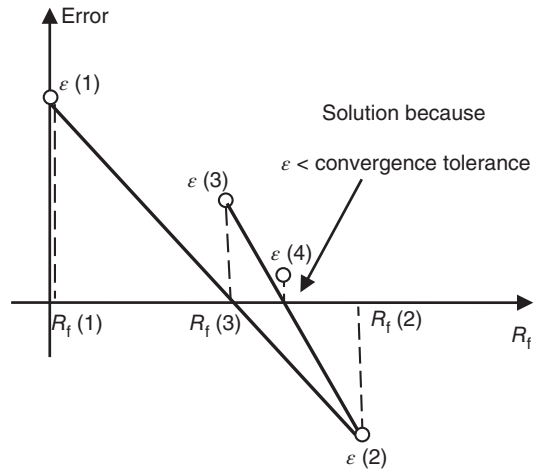


Figure 11. The procedure for estimating the fault resistance. Source: Lotfifard et al. (46).

The value of the fault resistance is changed according to Figure 11 until the value of ε becomes smaller than a predetermined threshold value.

Once the fault resistance is determined, the similarity of the simulated scenarios and the actual faulted condition is determined. The fault scenario (i.e., the fault location among the identified list of fault locations) that generates voltage and current signals at the installed meters throughout the feeder is selected as the actual location of the fault. The following index quantifies the similarity between the simulated and the actual fault case:

$$\text{Flag} = \frac{1}{\text{Error} + \Delta} \quad (82)$$

where

Δ is a small value to prevent division by zero

$$\text{Error} = \varepsilon_{\text{amplitude(V)}}^2 + \varepsilon_{\text{phase(V)}}^2 + \varepsilon_{\text{phase(I)}}^2 \quad (83)$$

where

$\varepsilon_{\text{amplitude(V)}}$ is the difference between the amplitude of the characteristic voltage of the recorded and simulated voltage sags

$\varepsilon_{\text{phase(V)}}$ is the difference between the phase angle of the characteristic voltage of the recorded and simulated voltage sags.

$\varepsilon_{\text{phase(I)}}$ is difference between the phase angle of the recorded and simulated current at the root node (i.e., substation).

The fault scenario among the determined short list of identified possible fault locations with highest flag value in equation 82 is the actual fault location.

Some of the influential factors on the accuracy of the algorithms are as follows:

- The accuracy of the parameters of the simulated/ modeled power distribution lines and tapped load values. This is because the proposed methods are model-based fault location algorithms that rely on the availability of the accurate model of the system.
- Uncertainties in the measured voltage and current signals by the meters.

- The type of the considered loads (i.e., constant impedance model or voltage-dependent model).

In Reference 45, a systematic approach is developed that quantifies the degree of the impacts of the abovementioned factors on the accuracy of different fault location methods.

8.3. Selection Criteria

Due to the importance of fault location identification, many fault location methods have been proposed in the past, and some of them were discussed in the previous sections. Different methods have strengths and shortcomings, depending on the considered assumptions and implementation requirements. A relevant question is how to select the best fault location method that is suitable for the distribution system under study?

Some methods only require current and/or voltage measurements at the substation, while other methods require voltage and/or current measurements along the feeder in addition to the substation data. The collected data from the feeder need to be synchronized (i.e., Micro-PMU should be used) in some methods, while other methods can operate based on unsynchronized data such as voltage measurements by power quality meters that do not necessarily provide synchronized samples. Some methods are based on time domain analysis and require sampled data, while others are based on the phasor domain analysis and only require phasor measurements. Some methods such as traveling wave methods require data acquisition systems with high sampling rates in the order of megahertz, while other methods can operate based on conventional data acquisition systems in the range of kilohertz sampling rates.

The considered model for the feeder is another factor that should be considered. Fault location identification methods can be developed based on the short- or long-line models. Some methods consider the presence of laterals and sublaterals and multiphase systems. The lines can be homogeneous or heterogeneous. Load models are also different and can be constant impedance model or voltage-dependent model. Considered resistance of the fault is another factor that should be considered as some methods are only suitable for bolted faults.

The abovementioned requirements and assumptions have direct impacts on the selection of the fault location method for the distribution system under study. For example, algorithms based on time-domain analysis require fast communication systems for collecting the data. However, they are suitable for fault scenarios that a full cycle of during-fault data are not available in the case of subcycle faults (47).

It is quite possible that several methods meet the requirements and limitations of the system. To select the most suitable method among the identified short list of methods, the accuracy of the method in finding the location of the fault can be selected as the metric. For instance, in Reference 45, uncertainty analysis is performed to select the most suitable method. The error in estimating the

fault location is defined as follows:

$$e = f(x_1, x_2, \dots, x_n) \quad (84)$$

where e is the fault location estimation error, $f()$ is the function that relates the inputs (x_i s) to the output (estimated fault location error), and x_i represents factors that affect the estimation results. For instance, x_1 is the measured voltage signal at the substation; x_2 is the measured current signal at the substation; x_3 is the line parameter; x_4 is the estimated load at each node; and x_5 is the fault resistance.

The above uncertainty analysis can be solved using different methods, including $2n+1$ point estimation method that is used in Reference 45. The method with error can be selected as the most suitable fault location method.

9. PREDICTION OF FAULT LOCATION

The main steps for building a fault-prediction model are as follows:

- Data preprocessing. The collected raw data comes with a number of problems, such as missing data, bad data (outliers), data duplicates, and time synchronization errors. In addition, datasets are not usually tailored for the specific application that is being developed. Thus, they may contain a large amount of irrelevant information or information provided in a wrong format/unit. All these issues are solved during the data preprocessing.
- Prediction target definition. Depending on the specific application we are working on and the available temporal and spatial scales of our data, we can choose a different prediction target. For example, we may want to focus on the prediction of probability of transmission line outage one hour in advance, or we may choose to predict probability of distribution transformer failure during a specific day. This selection will define the required spatial and temporal targets used for the next step – spatiotemporal data correlation. There is a trade-off between choosing temporal and spatial scales of input data and accuracy of the prediction model. If we choose to make prediction with data on smaller spatial resolution, we can expect the lower accuracy. For example, if we can make more accurate prediction of the expected outage probability on the level of one distribution feeder, then we can make on the level of one distribution pole.
- Spatiotemporal correlation of data. Fault-prediction model requires a merge of various datasets collected with different spatial and temporal resolutions. For example, vegetation maps can be created based on the imagery data collected once per year that come as raster files with 100 m spatial resolution covering a wide geographical area. On the other hand, weather parameters can be obtained from sparsely located points of land-based weather stations, with temporal resolution of 1 min. Network geographical map is presented as a set of points (for substations, towers, and equipment units such as transformers and insulators)

and polylines (network lines and feeders). Prior to the creation of the prediction model inputs, all the data must be spatiotemporally correlated to ensure that the right measurement values are associated with the specific time and location.

- Creation of prediction model inputs. The prediction models require as input a set of features, and if available a set of associated labels. For example, if we are looking into a historical vegetation outage that occurred on the distribution feeder, we want to collect all the measurements for that particular moment in time at the feeder location, such as weather parameters and vegetation indices, and group them into a set of input features. If we are doing classification, we assign a binary value as a label (“1” for the event, and “0” for normal operation).
- Selection and training of the prediction model. The next step is to select a type of a prediction model we want to use. If we are trying to predict whether or not there will be a fault, we can use binary classification models (such as random forest and logistic regression). On the other hand, if we are trying to predict a specific value of a parameter that may lead to the fault (for example, predicting the insulator strength), we may choose to use linear regression models instead. In this step, the created input training dataset is used to train the machine learning model. Machine learning algorithms have hyperparameters that need to be set to a value that ensures the convergence and high accuracy of the model.
- Evaluation and visualization of the prediction results. The last step is testing of the prediction model performances on an unseen set of data and visualization of the results. The split of the training and testing dataset can be done in different ways; for example, one may choose to use first 10 months of the year as a training dataset, and the last two months as a testing dataset, or the testing dataset may be selected by picking 20% of the data randomly over the whole period. The type of visualization of results is selected based on the requirements of the application user.

We demonstrate the capabilities and accuracy of different machine learning algorithms for fault prediction through four different examples, ranging from distribution to transmission, including prediction on different spatial scales (transmission line, distribution feeder, transmission tower insulators, and distribution transformer), and a variety of machine learning algorithms, some for classification and some for regression-based problems. Various methods that will be presented in Section 9.1 have accuracy ranging from ~ 0.75 – 0.80 in the case of distribution system applications to ~ 0.85 – 0.90 in the case of transmission system applications.

9.1. Prediction of Transmission System Faults Caused by Environmental Conditions

The knowledge from historical outage and weather data is used for the training of the machine learning model to provide accurate predictions of weather-related faults

in the transmission system 1–3 hours ahead (48). Since spatial proximity plays an important role when it comes to outage occurrence prediction, the data holds a certain spatial structure that needs to be considered. The required datasets include the historical outage data and the historical weather measurements and weather forecast for the following parameters: Wind Direction, Wind Speed, Wind Gust, Temperature, Dew Point, Relative Humidity, Pressure, Precipitation/Hour, and Present Weather Codes.

An ensemble-based model that can handle binary classification problems such as collaborative logistic ensemble classifier (CLEC) (48) is used for event detection. Consider the training dataset $D = \{z_1 = (\mathbf{x}_1, y_1), \dots, z_N = (\mathbf{x}_N, y_N)\}$ in which the constituents of \mathbf{X} and \mathbf{y} are organized into pairs. The bias-variance balancing objective function of CLEC is defined as

$$R_{\text{obj}}(h, D) = \sqrt{R_{\text{emp}}(h, D)^2 + d\text{Corr}(\ell(\cdot, h), z_{\text{trn}})^2} \quad (85)$$

where $R_{\text{emp}}(h, D) = 1/N \sum_{i=1}^N \ell(z_i, h)$ is the empirical risk of a model h w.r.t. D , and $d\text{Corr}(\ell(\cdot, h), z_{\text{trn}})$ is the distance correlation (49), a measure of statistical dependence between a value outputted by a given loss function $\ell(\cdot, h)$ and a random training example (observation) z_{trn} . Minimizing the first term in $R_{\text{obj}}(h, D)$ protects against underfitting, while minimizing the second term indirectly prevents from overfitting (50). As this study concerns a binary classification problem, the loss function is chosen to assess misclassifications, that is, $\ell(z_i, h) = I(y_i \neq h(\mathbf{x}_i))$, where I is an indicator function.

To discover hidden data substructures, CLEC employs multiple “local” logistic regression (LR) models. D is sampled uniformly M times using stratified sampling without replacement, thus generating M data subsets D^1, \dots, D^M of size ηN , where $\eta \in (0, 1)$. Each D^m is used to train a single LR component F_{D^m} . Upon training all the M components, the label of an unobserved substation $\mathbf{x}_s = [\mathbf{x}, \mathbf{v}]$ can be predicted as

$$\Phi_D(\mathbf{x}_s) = \text{sign} \left(\sum_{m=1}^M F_{D^m}(\mathbf{x}_s) \right) \quad (86)$$

As for the probability scores of Φ_D , they are taken to be the average of the probabilities estimated by the components F_{D^m} . Further, the components’ subsets are modified by allowing the components to exchange information across their subsets. The observations are exchanged among the components in a way that maximizes the difference between the values of R_{obj} , calculated before and after each exchange, that is,

$$(j^*, k^*) = \underset{(i,j)}{\text{argmax}} \Delta_{jk} = \underset{(i,j)}{\text{argmax}} R_{\text{obj}}(\Phi_D, D) - R_{\text{obj}}(\Phi_{D^{(jk)}}, D) \quad (87)$$

The CLEC algorithm was tested and compared to the logistic regression (LR) (48). The results are presented in Table 1 (48). We can observe that the CLEC algorithm outperforms LR. Figure 12 (48) presents the real-time outage probability maps. In ideal case, the predicted probability is high (red color) at the outage locations and low (dark green

Table 1. Prediction Performance w.r.t. Different Evaluation Metrics

Model	Acc.	AUC	F1	Bias
LR	0.85	0.93	0.81	0.68
CLEC	0.89	0.93	0.85	0.77

Source: Based on Dokic et al. (48).

color) everywhere else. The following can be observed from the map in Figure 12 (i) for the no-outage locations, the predicted probability of outages was less than 60%; (ii) for the cases with multiple outages in the network, the area with faults had points with high outage probability (over 80%).

9.2. Prediction Distribution System Faults Caused by the Surrounding Trees

We introduced the predictive data-driven method for vegetation management in distribution (51). The model enables real-time analysis of the vegetation impact on the distribution feeders based on predictive risk maps. Prediction algorithm is based on the Gaussian conditional random field (GCRF) regression predictor (52). The dataset used for the study is outlined in Table 2 (51).

A GCRF is used for the prediction of network vulnerability. The GCRF model uses a weighted graph as a data structure, which enables the exploitation of spatial similarities between the nodes for the improved prediction capability. The GCRF predicts the state of vegetation impact, denoted y , based on the historical measurements in the input vector \mathbf{x} . The GCRF expresses the conditional distribution as

$$P(\mathbf{y}|\mathbf{x}) = \frac{1}{Z} \exp \left(- \sum_{i=1}^N \sum_{k=1}^K \alpha_k (y_i - R_k(\mathbf{x}))^2 - \sum_{i,j}^L \sum_{l=1}^L \beta_l e_{ij}^{(l)} S_{ij}^{(l)}(\mathbf{x}) (y_i - y_j)^2 \right) \quad (88)$$

where Z is a normalization constant, x is a set of input variables from the historical measurements, y is a set of output variables, N is a total number of nodes (line sections) in the network graph, R_k are unstructured models where k is the number of predictors, S_{ij} represent similarities between outputs at nodes i and j determined based on their geographical distance, L is the number of branches, α are the parameters of the association, and β are the interaction potentials.

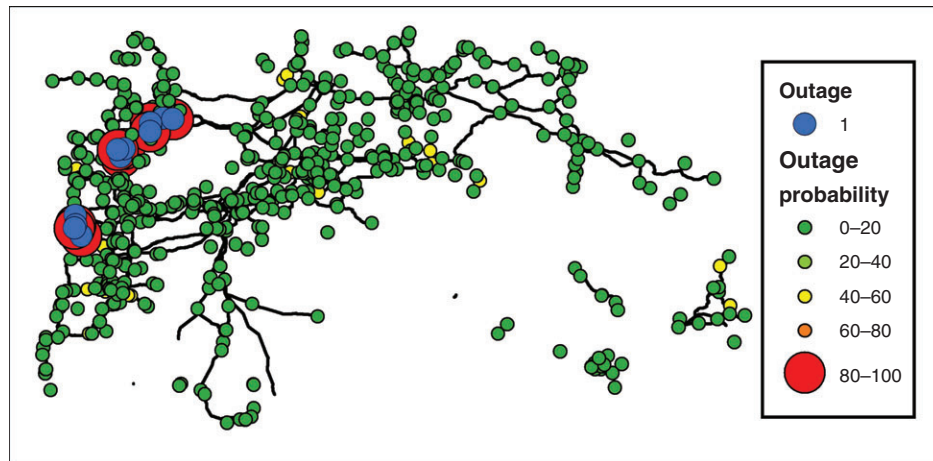

Figure 12. Example of predicted fault probabilities map. Source: Dokic et al. (48).

Table 2. Parameters Extracted in Preprocessing

	Historical outage data	Periodic tree trimming	Reactive tree trimming	Poles	Lines	Vegetation	Weather
Spatial	Point shapefile	Polyline shapefile	Polyline shapefile	Point shapefile	Polyline shapefile	Raster, polygon shapefiles	Points, polygon shapefiles
Temporal	Start and end time	Year quarter	Date	Static	Static	Year	1 min–3 h
Other parameters	Num. of customers, cause code	Trim period, num. of customers, cost	Cost	Material/class, height	Conductor size, count, and material, nominal voltage	Imagery, vegetation classes	Wind, temperature, precipitation, humidity, pressure, forecast ...

Source: Dokic and Kezunovic (51).

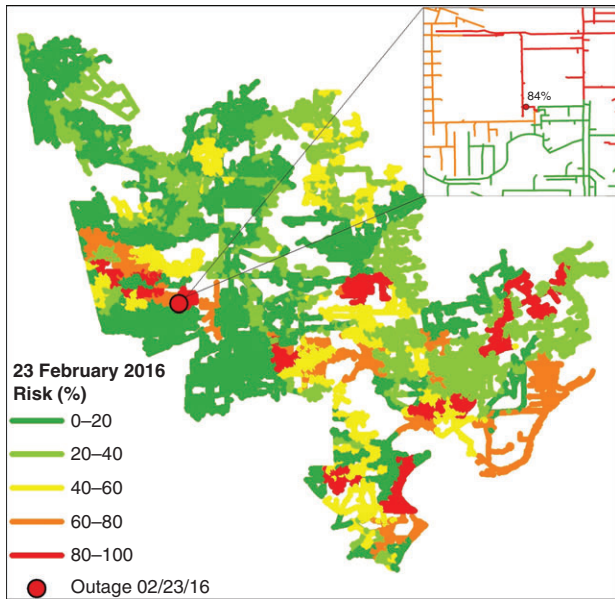


Figure 13. Example of vegetation risk map. Source: Dokic and Kezunovic (51).

The output y of the algorithm is the predicted state of vegetation impact on the feeder section. The parameters α and β from equation 88 can be estimated by maximizing the conditional log-likelihood from our training set and applying the gradient descent optimization algorithm:

$$L(\alpha, \beta) = \sum \log P(x) \quad (89)$$

$$(\alpha, \beta) = (L(\alpha, \beta)) \quad (90)$$

The benefits of this method are confirmed on an actual utility distribution network in Texas. The area of the analyzed network is $\sim 2000 \text{ km}^2$, containing approximately 200 000 poles and 120 000 feeders. The historical data were collected from January 2011 up to the end of April 2016. Over this period, 90% of the collected data were used for training of the prediction algorithm, while the remaining 10% of outages at the end of 2015 and beginning of 2016 were used as testing set. The predicted risk map for 23 February 2016 is presented in Figure 13 (51). We can observe that the predicted risk value on the faulted section is 84%.

9.3. Prediction of Distribution Transformer Failures

According to the study in Reference 53, weather and aging combined are a cause for over 50% of distribution transformer failures. In order to verify the correlation between weather parameters and DT failure, it is necessary to collect the historical weather and DT failure data. Then, the LR can be used to predict the probabilities of DT failures associated with the specific expected weather conditions. The DT failure study (53) analyses the weather impacts on step-down transformers (22.9 kV–220 V) used in the distribution sectors in South Korea.

Dataset used for the study contains the data for modeling outage events used for prediction and analysis starting

from year 2012 up to year 2018, a total of 237 events. The historical outages are extracted for five causes: lighting, tree contact, snow, rain, and dust. The weather parameters considered in this study are Lightning, Average Temperature, Highest Temperature (HT), Relative Humidity, Maximum Wind Speed, Wind Gust, and Precipitation. The dates that have outages caused by weather are selected for $Y = 1$, and the dates that do not have any outages are presented as $Y = 0$ and historical weather are extracted.

The LR model is used for modeling a binary response (i.e., success/fail). This model estimates the probability of the response occurring $P(X) = \Pr(Y = 1 | X)$ through a linear function of explanatory variables X . In this study, it is natural that the response variable Y is a DT failure, that is, 1 (failure) and 0 (no failure), and weather predictors are available for modeling LR. Specifically, X is $n \times (p + 1)$ design matrix, where n is the number of observations, and p is the number of weather predictors. Naturally, the number of coefficients is eight by seven predictors and an intercept. The corresponding coefficients β of the predictors designate the effect of the weather predictors on the probability of the DT failure. The basic intuition behind using maximum likelihood to fit a LR model is as follows: we seek estimates such that the predicted probability of failure for each individual DT is most likely to agree with its observed failure. This intuition can be formalized using the mathematical equations 91–93 as follows:

$$\beta = [\beta_0, \dots, \beta_7]^T \quad (91)$$

$$\ell(\beta) = \prod_{i:y_i=1} p(x_i) \prod_{i':y_{i'}=0} (1 - p(x_{i'})) \quad (92)$$

$$\hat{\beta} = \max_{\beta} \ell(\beta) \quad (93)$$

Once the coefficients in equation 93 have been estimated, the probability of failure is given by

$$p(x) = \frac{e^{x^T \beta}}{1 + e^{x^T \beta}} \quad (94)$$

To evaluate LR, the receiver operating characteristics (ROC) graphs and the area under curve (AUC) are used. The historical DT failure data are divided into the testing and training sets; 90% of the total dataset is selected for training, and the remaining 10% of the data are used for the testing. The degree of high temperature (HT) is classified into three temperature thresholds such as 82.4 °F, 86 °F, and 89.6 °F in order to make the interpretation of the HT coefficient precise. The model reported the AUC of 0.796, 0.798, and 0.764 for 82.4 °F, 86 °F, and 89.6 °F, respectively, as shown in Figure 14 (53).

9.4. Prediction of Transmission System Insulator Failures

We present here a predictive framework for mapping of insulator faults in the transmission network (54). Based on the observation of risk tracking and prediction, the zones with the highest probability of lightning caused outages are identified. A variety of data sources are used: utility asset management, geographical information system, lightning detection network, historical weather and

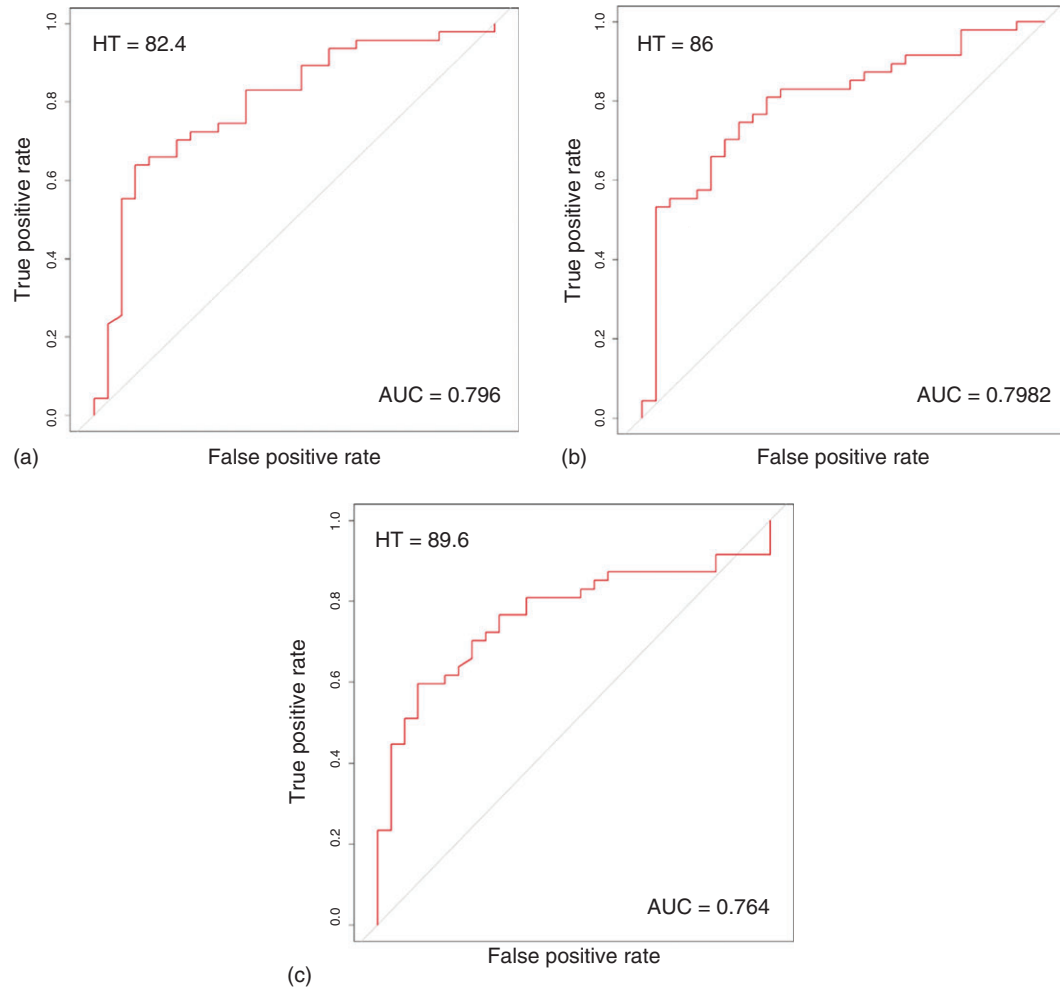


Figure 14. ROC for LR of DT failures. (a) HT = 82.4 °F; (b) HT = 86 °F; (c) HT = 89.6 °F. Source: Hui Ko et al. (53).

Table 3. List of Parameters

Historical network data	Insulator physical characteristics	In-field measurements		Weather parameters	Other environmental parameters
Outage reports	Surge impedances of towers and ground wires	Leakage current magnitude	Corona discharge detection	National lightning detection network	Vegetation index (presence and canopy height)
Maintenance orders	Footing resistance	Flashover voltage	Infrared reflection thermography	Automated surface observing system	Elevation
Replacement orders	Component BIL	Electric field distribution	Visual inspection reports	National digital forecast database	Soil

Source: Kezunovic et al. (54).

weather forecasts, and vegetation and soil properties, as outlined in Table 3 (54).

The proposed application is focused on predicting the risk of transmission line insulators experiencing an insulation breakdown due to the accumulated deterioration over time and an instant impact of a given lightning strike. The linear regression prediction-based algorithm, GCRF,

previously described in Section 8.3, observes the impact of various historical events on each individual component. In addition, the spatial distribution of various impacts is used to enhance the predictive performances of the algorithm.

For each lightning strike, the lightning protection parameters are calculated for the existing atmospheric

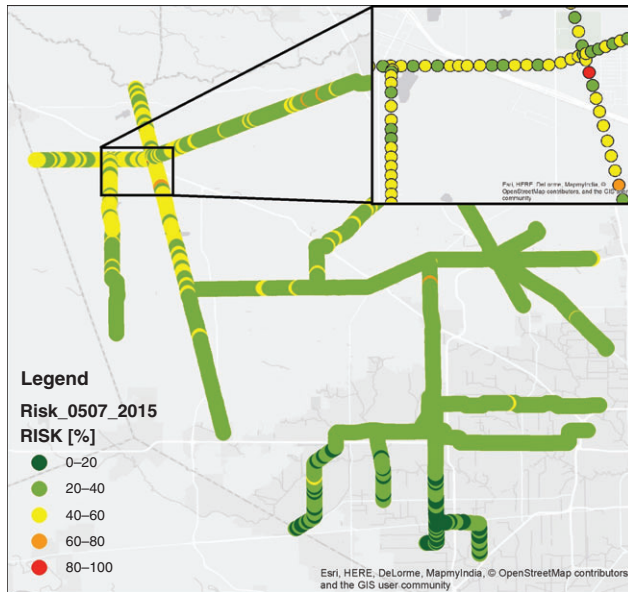


Figure 15. Example of insulator failure risk map. Source: Kezunovic et al. (54).

conditions obtained from the historical weather data. Additional weather parameters (temperature, humidity, pressure, and precipitation) are needed to calculate BIL under nonstandard atmospheric conditions (55). First, the relative air density and humidity correction factor are calculated as equation 95

$$\delta = \frac{PT_s}{P_s T}, H_c = 1 + 0.0096 \cdot \left[\frac{H}{\delta} - 11 \right] \quad (95)$$

where T_s and P_s are the standard temperature and pressure, respectively, and T and P are the measured temperature and pressure, respectively. The humidity correction factor is equal to 1 for rainy conditions, and for dry conditions it is calculated using equation 95. Then, the BIL under nonstandard atmospheric conditions is calculated as BIL_A :

$$BIL_A = \delta H_c BIL_S \quad (96)$$

where BIL_S is the standard BIL.

The method has been simulated and tested on a section of the network containing 36 substations and 65 transmission lines, with a total of 1590 towers. The historical outage and lightning data for the period of 5 years were observed. The risk map assigning insulator fault probability to each transmission line tower in the network is shown in Figure 15 (54).

10. CONCLUSIONS

While this survey gives an overview of many different approaches to fault location, it is by no means a comprehensive review. Over the years, the researchers have proposed many variants of the algorithms, with some extending the ideas given in this overview. The IEEE Standards Organization has also issued a thorough

overview that is highly recommended since it covers many practical implementation aspects (56).

We have covered only some selected approaches that we felt our most critical to understanding the application issues or to appreciate some new approaches to solving the fault location problem.

In the final assessment of the fault location algorithms that we have covered, several observations are quite relevant for the understanding of the approaches and their future implementation:

- In all fault location applications, one has to balance a delicate trade-off between accuracy and an effort in collecting and processing the required data. The implementation method is directly tied to the type of data required.
- Achieving high accuracy is always a goal, but the cost of implementation may be prohibitive for some of the proposed methods. To select the best approach, a study of the value of an accurate fault location is needed.
- An important differentiation in considering the needed data is to assess whether the data is readily available, or additional study time or cost need to be incurred for obtaining the data. If the data is available but not readily accessible, then it is one-time cost to make it ready for the use in fault location.
- Another important component is the type of measurements needed to implement the algorithm. If the measurements can be obtained from the devices that are already installed, then this is a major advantage since the device installation and utilization cost that is already invested is leveraged.
- Last but not the least, the speed with which the fault location may be determined may also matter. In the instances when the operators can take an immediate control action if the fault location is known, the real-time calculation of fault location may be invaluable.

BIBLIOGRAPHY

1. P. F. Gale P. Crossley, X. Bingyin, G. Yaozhong, B. Cory, and J. Barker. Fault Location Based on Traveling Waves, in *Proc. 5th Int. Conf. Develop. Power Syst. Protection*, pp 54–59; IEE, 1993.
2. R. E. Willson. *IEEE Trans. Power Deliv.* **1992**, 7, pp 126–132.
3. B. Perunicic, A. Y. Jakwani, and M. Kezunovic. An Accurate Fault Location on Mutually Coupled Transmission Lines Using Synchronized Sampling, in *Stockholm Power Tech. Conf.*, Stockholm, Sweden, 1995.
4. T. Takagi, Y. Akimoto, T. Yamamoto, H. Hosakawa, T. Sakaguchi, T. Yoshida, and S. Nishida. Fault Protection Based on Traveling Wave Theory: Part I, Theory, in *IEEE PES Summa Power Meet.*, 1977.
5. M. S. Sachdev and R. Agarval. *IEEE Trans. Power Deliv.* **1988**, 3, pp 121–129.
6. D. Novosel. Accurate Fault Location Using Digital Relays, in *Int. Conf. Power Syst. Technol.* Beijing, China, 1994.
7. A. A. Girgis, D. G. Hart, and W. I. Peterson. *IEEE Trans., Power Deliv.* **1992**, 7, pp 98–107.

8. R. Courant and F. John. *Calculus and Analysis*, vol. 2. Wiley-Interscience: New York, 1974.
9. Xiangqing Jiao and Yuan Liao. A Linear Estimator for Transmission Line Parameters Based on Distributed Parameter Line Model, in *Power and Energy Conference at Illinois*, Champaign, IL, February 23–24, 2017.
10. W. Xiu and Y. Liao. *Int. J. Emerg. Electr. Power Syst.* **2014**, 15(6), pp 513–526.
11. P. Ren, A. Abur, and H. Lev-Ari. Tracking Transmission Line Parameters in Power Grids Observed by PMUs, in *2019 IEEE Milan PowerTech*, Milan, Italy.
12. V. Milojevic, S. Calija, G. Rietveld, M. V. Acanski, and D. Colangelo. *IEEE Trans. Instrum. Meas.* **2018**, 67(10), pp 2453–2462.
13. P. K. Mansani, A. Pal, M. Rhodes, and B. Keel. Estimation of Transmission Line Sequence Impedances Using Real PMU Data, in *2018 North American Power Symposium*, NAPS 2018, pp 1–6, 2019.
14. Yiqi Zhang and Yuan Liao. Kalman Filter Approach for Line Parameter Estimation for Long Transmission Lines, in *Power and Energy Conference at Illinois*, Champaign, IL, USA, Feb. 20–21, 2020.
15. L. Collatz. *The Numerical Treatment of Differential Equations*. Springer-Verlag: New York, 1960.
16. J. Kohlas. Estimation of Fault Location on Power Lines, in *3rd IFAC Symp., Hague/Delft*, The Netherlands, pp 393–402, 1973.
17. A. O. Ibe and B. I. Cory. *A Traveling Wave-Based Fault Locator for Two- and Three-Terminal Networks*. *IEEE Ind. Comput. Appl. Conf.* San Francisco, 1985.
18. G. B. Ancell and X. C. Pahalawatha. *IEEE Trans., Power Deliv.* **1994**, 9, pp 680–689.
19. F. L. Alvarado, S. K. Mong, and M. K. Enns. *IEEE Trans. Power Appar. Syst.* **1985**, PAS-104(5), pp 1109–1120.
20. Computer-Aided Protection Engineering User Documentation, Siemens Industry, Inc.
21. A. T. Giuliante, D. M. Mac Gregor, A. M. Makki, and A. P. Napikoski. Using Event Recordings to Verify Protective Relay Operations, in *Georgia Tech Fault and Disturbance Analysis Conference*, Atlanta, Georgia; May 5–6, 2003.
22. J. A. Jiang, J.-Z. Yang, Y.-H. Lin, and C.-W. Liu. *IEEE Trans. Power Del.* **2000**, 15(2), pp 486–493.
23. J. A. Jiang, J.-A. Jiang, Y.-H. Lin, J.-Z. Yang, T. Too, and C.-W. Liu. *IEEE Trans. Power Del.* **2000**, 15(4), pp 1136–1146.
24. Y. H. Lin, C.-W. Liu, and C.-S. Chen. *IEEE Trans. Power Del.* **2004**, 19(4), pp 1587–1593.
25. Y. H. Lin, C.-W. Liu, and C.-S. Chen. *IEEE Trans. Power Del.* **2004**, 19(4), pp 1594–1601.
26. Y. Liao. *IEEE Trans. Power Del.* **2008**, 23(2), pp 609–617.
27. M. Korkali, H. Lev-Ari, and A. Abur. *IEEE Trans. Power Syst.* **2012**, 27(2), pp 1003–1011.
28. M. Korkali and A. Abur. *IEEE Trans. Power Syst.* **2013**, 28(1), pp 482–489.
29. Y. Chen, D. Liu, and B. Xu. *IEEE Trans. Smart Grid* **2013**, 4(2), pp 1207–1215.
30. S. Azizi, M. Sanaye-Pasand, M. Abedini, and A. Hassani. *IEEE Trans. Power Del.* **1999**, 14(3), pp 863–867.
31. J. S. Thorp, C. Seyler, and A. Phadke. *IEEE Trans. Circuits Syst. I, Fundamental Theory Appl.* **1998**, 45(6), pp 614–622.
32. A. Semlyen. *IEEE Trans. Power App. Syst.* **1974**, PAS-93(2), pp 676–684.
33. P. Dersin and A. Levis. *IEEE Trans. Power App. Syst.* **1982**, PAS-101(1), pp 60–70.
34. A. J. Arana. Analysis of Electromechanical Phenomena in the Power-Angle Domain. PhD dissertation, Elect. Eng. Dept., Virginia Polytechnic Institute and State University, Blacksburg, VA, USA, Dec. 2009.
35. M. Parashar, J. S. Thorp, and C. E. Seyler. *IEEE Trans. Circuits Syst. I, Reg. Papers* **2004**, 51(9), pp 1848–1858.
36. E. W. Dijkstra. *Numer. Math.* **1959**, 1, pp 269–271.
37. D. K. Ranaweera. *Elect. Power Syst. Res.* **1994**, 29, pp 99–104.
38. R. Das, M. S. Sachdev, and T. S. Sidhu. A Fault Locator for Radial Subtransmission and Distribution Lines, in *IEEE Power Engineering Society Summer Meeting*, Seattle, WA, 1, pp 443–448, 2000.
39. J. Zhu, D. L. Lubkeman, and A. A. Girgis. *IEEE Trans. Power Del.* **1997**, 12(2), pp 801–809.
40. Z. Q. Bo, G. Weller, and M. A. Redfern. *IEE Proc. Gener. Transm. Distrib.* **1999**, 146(1), pp 73–79.
41. J. J. Mora, G. Carrillo, and L. Perez. Fault Location in Power Distribution Systems Using ANFIS Nets and Current Patterns, in *IEEE PES Transmission and Distribution Conference and Exposition Latin America*, Caracas, Venezuela, 2006.
42. S. Lotfifard, J. Faiz, and M. Kezunovic. *Electr. Power Syst. Res.* **2012**, 91, pp 1–8.
43. I. Kiaei and S. Lotfifard. *IEEE Trans. Smart Grid* **2020**, 11(1), pp 74–83.
44. M. Farajollahi, A. Shahsavari, E. M. Stewart, and H. Mohsenian-Rad. *IEEE Trans. Power Syst.* **2018**, 33(6).
45. S. Lotfifard, M. Kezunovic, and M. J. Mousavi. *IEEE Trans. Power Del* **2013**, 28(01), pp 285–293.
46. S. Lotfifard, M. Kezunovic, and M. J. Mousavi. *IEEE Trans. Power Del.* **2011**, 26(2), pp 1239–1246.
47. C. J. Kim, and T. O. Bialek. Sub-Cycle Ground Fault Location — Formulation and Preliminary Results, in *IEEE/PES Power Systems Conference and Exposition (PSCE)*, pp 1–8, Mar. 2011.
48. T. Dokic, M. Pavlovski, D. Gligorijevic, M. Kezunovic, and Z. Obradovic. *Spatially Aware Ensemble-Based Learning to Predict Weather-Related Outages in Transmission*, HICSS 2019. Maui: Hawaii, 2019.
49. G. J. Székely, G. J. Székely, M. L. Rizzo, and N. K. Bakirov. *Ann. Stat.* **2007**, 35(6), pp 2769–2794.
50. M. Pavlovski, F. Zhou, N. Arsov, Lj. Kocarev, and Z. Obradovic. Generalization-Aware Structured Regression towards Balancing Bias and Variance. IJCAI. 2018.
51. T. Dokic and M. Kezunovic. *IEEE Trans. Smart Grid* **2018**, 10(5), pp 4776–4785. doi: 10.1109/TSG.2018.2868457.
52. V. Radosavljevic, S. Vucetic, and Z. Obradovic. Neural Gaussian Conditional Random Fields, in *Proc. European Conference on Machine Learning and Principles and Practice of Knowledge Discovery in Databases*, Nancy, France, 2014.
53. E. Hui Ko, T. Dokic, and M. Kezunovic. Prediction Model for the Distribution Transformer Failure using Correlation of Weather Data, in *5th International Colloquium “Transformer Research and Asset Management”* Opatija, Croatia, 2019.
54. M. Kezunovic, T. Dokic, and R. Said. Optimal Placement of Line Surge Arresters Based on Predictive Risk Framework Using Spatiotemporally Correlated Big Data, at *CIGRE General Session*, Paris, France, Aug. 2018.

55. A. R. Hileman. *Insulation Coordination for Power Systems*. CRC Taylor and Francis Group: LLC, 1999.
56. IEEE Std C37.114-2014. IEEE Guide for Determining Fault Location on AC Transmission and Distribution Lines, 2014.

MLADEN KEZUNOVIC
TATJANA DOKIC
Texas A&M University, TX, USA

Ahad Esmailian
Avangrid Orange, CT, USA

Ashok Gopalakrishnan
Siemens Industry, Ann Arbor, MI, USA

Yuan Liao
The University of Kentucky Lexington, KY,
USA

Saeed Lotfifard
Washington State University Pullman, WA,
USA